Seismicity and the State of Stress in the Dezful Embayment, Zagros Fold and Thrust Belt

Ali Yaghoubi*[1], SeyedBijan Mahbaz[1, 2], Maurice B. Dusseault[1, 2], Yuri Leonenko[1,3]

[1]Department of Earth and Environmental Sciences, University of Waterloo, Waterloo, ON N2L 3G1, Canada

[2]Waterloo Institute for Sustainable Energy (WISE), University of Waterloo, Waterloo, ON N2L 3G1, Canada

[3]Department of Geography and Environmental Management, University of Waterloo, Waterloo, ON N2L 3G1, Canada

Abstract

This study focuses on determining the orientation and constraining the magnitude of the present-day stress in the Dezful Embayment in Iran's Zagros Fold and Thrust Belt. Two datasets are used: the first includes petrophysical data from 25 wells (3 to 4 km), and the second contains 108 earthquake focal plane mechanisms mostly occurring in blind active basement faults (5 to 20 km). Formal stress inversion analysis of the focal plane mechanism demonstrates that the major basement faults are reverse faults with $S_{Hmax} > S_{hmin} \cong S_v$ (A_ϕ=2.0-2.2). The seismologically determined S_{Hmax} direction is 37°±10°, nearly perpendicular to the strike of most faults in the region. However, borehole geomechanics analysis using rock strength and drilling evidence leads to the counterintuitive result that the shallow state of stress is a normal/strike-slip regime. These results are consistent with the low seismicity level in the sedimentary cover in the Dezful Embayment, and may be evidence of stress decoupling due to the existence of salt layers. This finding also aligns with the Mohr-Coulomb faulting theory in that the N-S strike-slip basement Kazerun fault has an unfavourable orientation for slip in a reverse fault regime with an average SW-NE S_{Hmax} orientation. The stress state situation in the field was used to identify the optimally oriented fault planes and the fault friction factor. For each focal plane mechanism, the ratio of shear to effective normal stress (the required frictional coefficient) was used to determine a geometrically preferred slip plane. The results are useful for determining the origin of seismic activity in the basin and better assessing fault-associated seismic hazards in the area.

Keywords: Focal mechanisms, Fault Mechanics, Seismicity, Stress State, Dezful Embayment, Zagros Fold and Thrust Belt.

1. Introduction

The Zagros fold-and-thrust belt (ZFTB), southwest Iran, is one of the most seismically active areas in the world (Berberian, 1995; Talebian and Jackson, 2004), with more than 5000 earthquakes with $M_w \geq 3$ recorded between January 1, 2010, and January 1, 2020 (Iranian Seismological Centre). The Dezful Embayment (DE) within the ZFTB is also one of the richest hydrocarbon regions in the world, hosting many onshore hydrocarbon fields and containing about 9% of global hydrocarbon (Bordenave and Hegre, 2010). Improving our knowledge of its state of stress is important, in view of the area's enormous economic value and seismic activity.

Understanding the state of stress in the area is important to seismology research (Hauksson, 1994; Levandowski et al., 2018) and to reservoir geomechanics studies at various scales (Dusseault, 2011). Knowing the state of stress in the DE helps us understand crustal-scale seismicity pattern issues (10 km) arising from oil and gas extraction (McGarr et al., 2002), the reservoir scale issues (1 km) of induced seismicity (Shen et al., 2019), and borehole scale engineering issues (10 m) related to casing shear and borehole stability (Dusseault et al., 1998). In the DE area, most seismicity occurs around the Balarud Fault (BL), Kazerun Fault (KZ), and the Mountain Front Fault (MFF), and is restricted to below 6 km and to a surface elevation of fewer than 1500 m above sea level (Figure 1). However, the major oil and gas fields of the DE region are located at low elevation; therefore, combining both earthquake datasets and borehole well logs leads to better coverage of the various scales.

Numerous studies have focused on determining stress state using earthquake focal mechanism data in the ZFTB, where most seismicity happens on blind faults at basement level or beneath the sedimentary cover at depths of 5-20 km (Allen et al., 2013; Allen and Talebian, 2011; Berberian, 1995; Jackson and Fitch, 1981; Lacombe et al., 2006; Nissen et al., 2011; Sarkarinejad et al., 2017; Talebian and Jackson, 2002, 2004; Tatar et al., 2004; Zarifi et al., 2014). Berberian (1995) stated that active thrust basement fault systems are covered by quiescent sedimentary layers in the ZFTB. A micro-earthquake study (Yamini-Fard et al., 2006) carried out around the Kazerun fault systems also revealed that the shallower sedimentary cover deforms by strike-slip faulting, but that a reverse faulting regime exists at greater depths(>7km). However, very few studies have integrated drilled wellbore datasets for shallower depths (<5 km) to help delineate the area's current state of stress (Haghi et al., 2018; Yaghoubi and Zeinali, 2009). The study by Yaghoubi and Zeinali (2009) in the Cheshmeh-khosh field and by Haghi et al. (2018) in the Mansouri field indicated that normal/strike-slip faulting predominates in the sedimentary cover to a depth of 5 km.

The presence of several continuous highly ductile layers in the ZFTB leads the upper sedimentary cover to be decoupled form the basement (Mouthereau et al., 2007). The state of stress in the DE is a classic case of decoupling, where the stress regimes are changed at different depth because of the existence of highly ductile layers. These ductile zones shield the shallower sediments from the compressional strains in the basement rock arising from the collision between the Arabian and Eurasian plates that have generated the Zagros (Bahroudi and Koyi, 2003; Berberian, 1995; Molinaro et al., 2005; Sepehr and Cosgrove, 2004; Walpersdorf et al., 2006).

This study determines the orientation and constrains the magnitude of the area's present-day stresses and faulting regimes (e.g., normal, strike-slip, or reverse) based on geophysical wellbore log datasets of 25 wells as well as 108 earthquake focal plane mechanisms. The database includes the style of faulting derived from earthquake focal mechanism and analyses of borehole breakouts and tensile induced fractures. Evidence of stress-induced borehole instability and geophysical data from various wells as well as seismicity datasets are also used to estimate the state of stress in the DE.

2. Regional Tectonic Setting

The Zagros Fold and Thrust Belt (ZFTB) results from the active collision of Arabian and Eurasian plates. Extending for almost 1400 km and 100-200 km wide, with an approximately N125°-160° trend, it stretches from eastern Turkey to the northern area of the Strait of Hormuz in the Persian Gulf. The ongoing collision started during the Miocene era as the Arabian plate pushed against central Iranian (Berberian, 1995). This compressional tectonic activity has led to significant crustal shortening across the fold belt, and resulted in faulting and folding, thrusting, and reactivation of large-scale strike-slip faulting of the sedimentary cover sequence (Agard et al., 2005; Alavi, 1994). Among the major faults are the Izeh-Hendijan Fault (IZHF), the Kharg-Mish Fault (KMF), and the Kazerun Fault (KZ) (Figure 1).

The deep-seated strike-slip Balarud Fault (BF) from the northwest and the Kazerun Fault from the southeast divide the ZFTB into different geological zones, each with a different structural style and stratigraphy. These zones include two regional embayments: the Kirkuk Embayment to the northwest and the Dezful Embayment (DE) to the southeast. There are also folded belts: from NW to SE, the Lorestan, Izeh and Fars (Central Zagros) provinces (Sepehr and Cosgrove, 2007). An earlier study by Sherkati and Letouzey (2004) showed that the DE has subsided approximately 5000 m compared to the Izeh zone across the Mountain Front Fault (MFF).

Extending over 60,000 km^2, the DE is a discrete structural lowland bounded by the Balarud Fault and the Mountain Front Fault (MFF) to the north and northeast, the Kazerun-Borazjan Fault (KF) to the east and southeast, and the Zagros Foredeep Fault (ZFF) to the south and southeast. This embayment is one of the most prolific oil regions in the world (Bordenave and Burwood, 1995) and hosts more than 40 onshore hydrocarbon fields. Most of the hydrocarbon fields (oval green shape in Figure 1) are elongated along the regional strike of the whaleback folds, NW-SE, orthogonal to the shortening direction (SW-NE). The majority of oil and gas hydrocarbon fields in the DE are found in two regional carbonate zones, the Asmari and the Sarvak Formations. Most seismicity in the area occurs around the Balarud Fault (BL), Kazerun Fault (KZ), and the Mountain Front Fault (MFF). Each coloured dot in Figures 1 indicates the epicenter of an earthquake recorded by the Iranian Seismological Centre (IRSC) after 2010. We display that earthquakes have a recorded waveform only for the sake of accuracy (Table S1 in the supplementary materials).

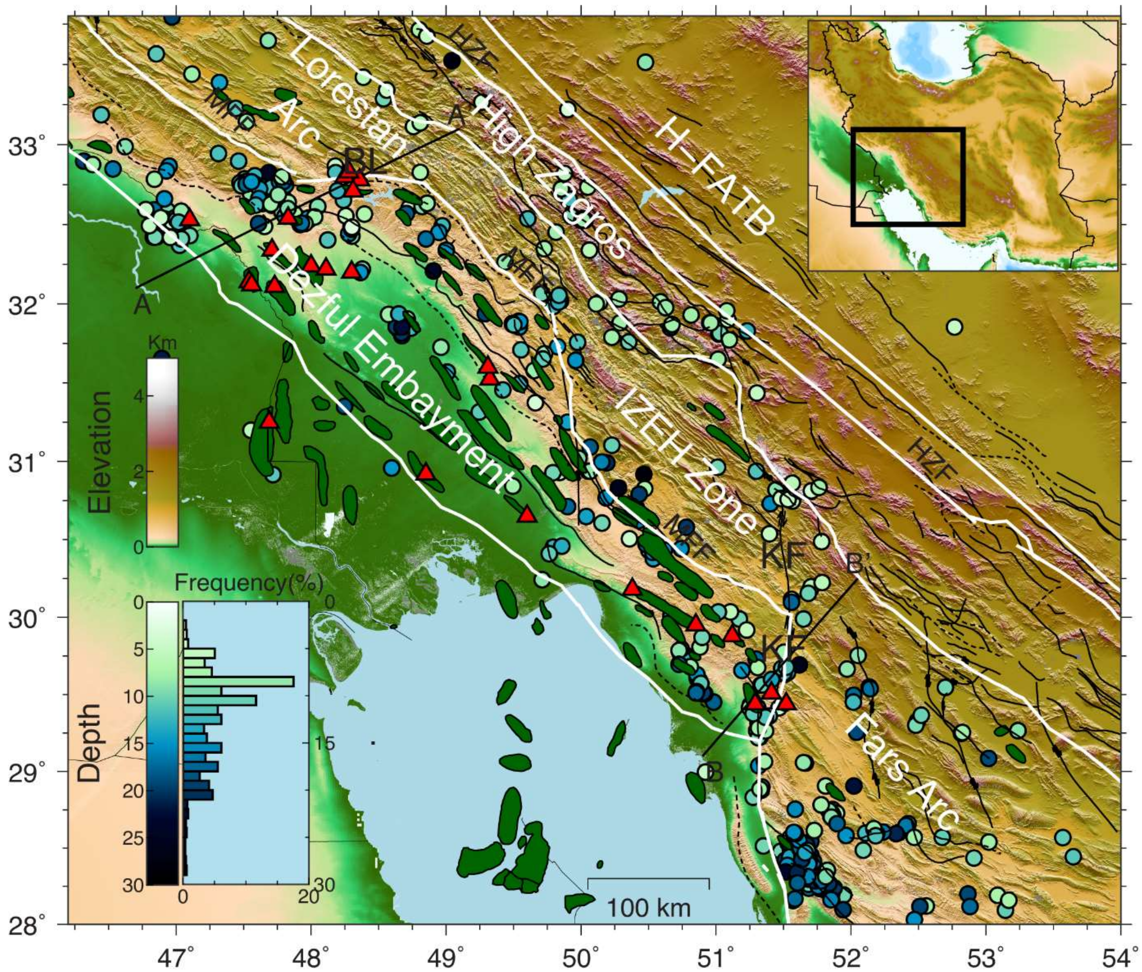

Figure 1: Topographic, structural and seismicity map of Zagros Fold and Thrust Belt along with locations of hydrocarbon fields (green oval shape). Coloured circles are IRSC-recorded earthquake centroid depths since 2010. Details of each earthquake are provided in the supplementary materials (Table S1). The bottom left histogram shows the depth distribution of earthquakes. Red triangles denote the location of the 25 wells investigated in this study. A-A′ and B-B′ are cross-sections of the seismicity and topography shown in Figure 5. Fault traces (the solid black lines) are inferred and compiled from Berberian (1995) and Talebian & Jackson (2004). The white lines show main structural subdivisions of the ZFTB. Major active faults are the HZF, High Zagros Fault; KZ, Kazerun Fault; MFF, Mountain Front Fault; MRF, Main Recent Fault; MZRF, Main Zagros Reverse Fault; ZFF, Zagros Foredeep Fault; BL, Balarud fault.

3. Dezful Embayment Stratigraphy

The present-day stratigraphic disposition of the Zagros Mountains and the DE is well established and is the result of a long geological history (Alavi, 1994, 2004, 2007; Bahroudi and Koyi, 2003; Bahroudi and Koyi, 2004; Fakhari et al., 2008; Jahani et al., 2007; James and Wynd, 1965; Mobasher and Babaie, 2008; Motiei, 1994; Pirouz, 2018; Pirouz et al., 2011;

Sherkati and Letouzey, 2004). Selected highlights of the DE stratigraphy are set out in the following two paragraphs.

More than 10 km of Palaeozoic sedimentary successions have been deposited over the infra-Cambrian Hormuz in the ZFTB. The significant difference in the stratigraphy between the DE and Fars geological province is that the sedimentary cover of Fars province has been deposited on top of the infra-Cambrian Hormuz Salt layer, whereas this layer is much thinner or absent in the north Zagros (Jahani et al., 2007). The main detachment levels in the DE are located in the evaporite-rich Triassic Dashtak and Mesozoic Gachsaran Formations (the yellow formations in Figure S1 of the supplementary materials).

The Gachsaran Formation (lower Fars) varies in thickness from several hundred to 2000 m and includes thick beds of evaporates (anhydrite, gypsum, and salt) with some marl, limestone, dolomite and shale zones (Bahroudi and Koyi, 2004; James and Wynd, 1965). The Gachsaran Formation is a regional seal and is the caprock for the Asmari Formation reservoirs. The Asmari Formation is composed of sandstone in its lower part and carbonates in the upper part (Figure S1), but at the northern edge of the basin, its uppermost part is conglomeratic with clasts derived from the Asmari itself (Mahbaz et al., 2011; Sardar and Mahbaz, 2009). The Upper Cretaceous Sarvak Formation, the second-most important reservoir unit in the DE, is part of the carbonate series of the Sarvak and Ilam Formations (Mahbaz et al., 2011) and overlain by the Gurpi Formation. Motiei (1994) pointed out that the Sarvak Formation consists of three limestone units, together reaching a maximum thickness of 821 m in the DE. The high hydrocarbon productivity of these reservoirs, particularly the Asmari, results mostly from the fracture systems created by the compressive folding characteristic of the Zagros area (Bordenave and Hegre, 2010).

4. Data Collection

Twenty-five wells were examined in our state of stress analysis of the DE. Comprehensive logging data and daily drilling report for the vertical section is available for all wells and includes their image logs. Detailed analysis of these logs has provided a circumferential (360°) picture of the borehole walls based on resistivity or acoustic contrast between fluid and rock. We have examined the drilling-induced wellbore failures, that is, the borehole breakouts and tensile-induced fractures, in all wells. Details of each well, including the depth of their image logs, are provided in Table 1. Red triangles in Figure 1 denote the locations of the examined wells, which were drilled in 15 different hydrocarbon fields at various locations in the DE.

A total of 108 individual well-constrained focal mechanisms have been extracted and compiled from previous publications and sources (Adams et al., 2009; Baker et al., 1993; Jackson and Fitch, 1981; Jackson and McKenzie, 1984; Maggi et al., 2000; McKenzie, 1972; Ni and Barazangi, 1986; Nissen et al., 2011; Peyret et al., 2008; Priestley et al., 1994; Skirokova, 1967; Talebian and Jackson, 2004) and the Iranian Seismological Centre (IRSC). Details of each focal mechanism and its references are provided in the supplementary materials. We have selected only those focal mechanisms that rank A in their references. Of the 108 focal mechanism, 73 are compiled from the IRCS using broad-wave forms modelling (Hosseini et al., 2019). The selected focal mechanisms range in depth from 5 to 20 km, with an average depth of 10 km. A number of the focal mechanisms belong to the Lorestan Arc and Fars Arc to evaluate the state stress variation on the border of structural subdivisions. Of all earthquakes considered in this focal mechanism study, 86 occurred in response to a thrust faulting regime at various locations, and 22 were triggered by a strike-slip regime that mostly occurred around the NS striking Kazerun Fault.

5. Constraining the state of stress form borehole data

5.1 Methodology

Since most of the ZFTB's earthquakes have been recorded below a depth of 5 km, datasets obtained from boreholes fill a critical gap in understanding the state of stress at shallower depths in the sedimentary cover. There are well-established techniques for determining stress orientation from borehole geometry and borehole geophysics datasets (Bell and Gough, 1979; Plumb and Cox, 1987). Drilling causes stress concentrations around borehole wall. The local stress concentrations due to drilling a circular hole in an infinite homogenous rock mass can be calculated form the Kirsch solution (Jaeger et al., 2009). In a vertical wellbore, observation of compressive features (breakouts) and tensile features (induced axial fractures) proves to be an effective approach for determining the minimum and maximum horizontal in-situ stress orientation respectively (Mastin, 1988; Schmitt et al., 2012).

In the context of the Mohr-Coulomb theory and considering Kirsch equation, compressive and tensile failure will occur when the stress tangential effective stress ($\sigma_{\theta\theta}$) or the vertical effective stress (σ_{zz}) exceeds the effective rock strength

$$\sigma_{\theta\theta} = S_{Hmax} + S_{hmin} - 2(S_{Hmax} + S_{hmin})\cos 2\theta - 2P_p - \Delta P \geq rock\ stength$$

$$\sigma_{zz} = S_V - 2\nu(S_{Hmax} - S_{hmin})\cos 2\theta - P_p \geq rock\ stength$$

$$\sigma_{rr} = \Delta P \quad (1)$$

where S_v, S_{Hmax}, S_{hmin} are vertical, maximum, and minimum horizontal stress magnitude respectively; ν is the static Poisson's ratio; Pp is pore pressure; and ΔP is differential borehole fluid pressure. Breakouts occur at the wellbore wall due to stress anisotropy and when the stress concentration exceeds the rock strength. Therefore, knowing the rock strength helps in placing a constraint on the state of stress.

The Leak-Off-Test (LOT), Hydraulic Fracturing Test and as well as Pressure While Drilling (PWD) (Ward and Andreassen, 1997) are different direct in-situ stress measurements taken during well drilling. An alternate approach used to constrain the in-situ stress magnitude in the absence of direct stress measurement is to consider that the stress magnitudes are in equilibrium with the frictional strength of pre-existing faults (Jaeger et al., 2009). The ratio of the maximum (S_1-P_P) to minimum (S_3-P_P) effective stress on a well-oriented cohesionless fault is limited by frictional strength:

$$(S_1 - P_p)/\,(S_3 - P_p) = \left[\sqrt{1+\mu^2} + \mu\right]^2 \quad (2)$$

where P_P is pore pressure and μ is the coefficient of frictional sliding on a pre-existing fault (Jaeger et al., 2009). The assumption is that one of the principal stresses is vertical. It has been found in laboratory studies and in-situ experiments that the magnitude of the coefficient of friction falls within the range of 0.6 to 1 (Townend and Zoback, 2000).

Although many boreholes have been drilled in the ZFTB area, Leak-Off-Tests (LOT) and hydraulic fracturing experiments have been performed only in some of them. Since no direct S_{hmin} measurement was available for this study, the state of stress had to be constrained from the borehole well logs data at the lower depth of the DE. Hence, bounds had to be established on the stress magnitudes using wellbore wall observations.

5.2 Stress Orientation

Detailed analysis was done on the image logs of 25 wells. Figure 2 illustrates examples of a) borehole breakouts, and b) and c) tensile induced fractures detected in different hydrocarbon fields located in the DE. Figure 3 shows the depth, frequency, and orientations of borehole breakouts in well PYW-7. Statistical analysis indicates that the S_{hmin} direction (borehole breakout azimuth) in well PYW-7 is 100.7°±5.7°. This result is approximately the same as that for the borehole breakout azimuth analysis in PYW-6, drilled about 4 km away (101.7°±12.1°). The same analysis was performed for different wells in the Paydar, Agha-Jari, Khaviz, Abe-Teymor, Lali, Marun, Dalpari, Cheshmeh-khosh, and Mansori fields. The S_{Hmax} orientations resulting from breakouts, plus the tensile-induced fractures in each well, are ranked A to D according to the World Stress Map quality ranking system (Heidbach et al., 2016; Heidbach et al., 2010). Table 1 presents the result of this analysis of borehole breakouts and tensile-induced fractures in different fields in the DE.

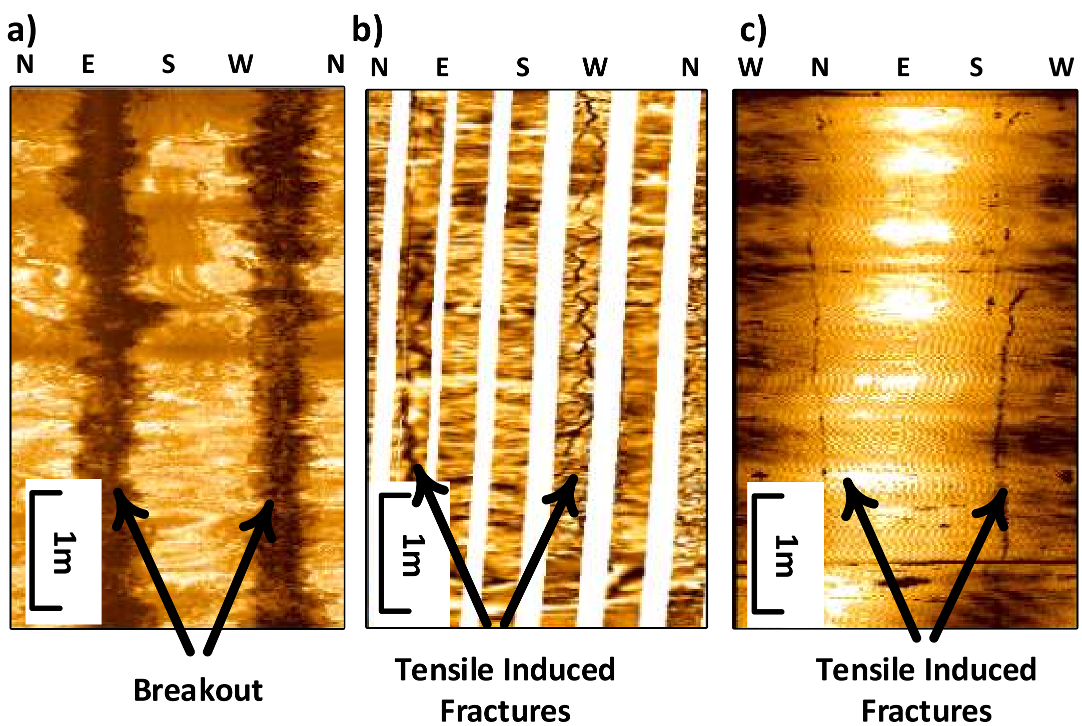

Figure 2: Examples of borehole breakout in a) the E-W direction in the Dehloran oil field (4150 m) and b) tensile induced fracture in NE-SW direction in the Khesht oil field (2880 m), and c) one in the N-S direction in the Paydar oil field (3210 m).

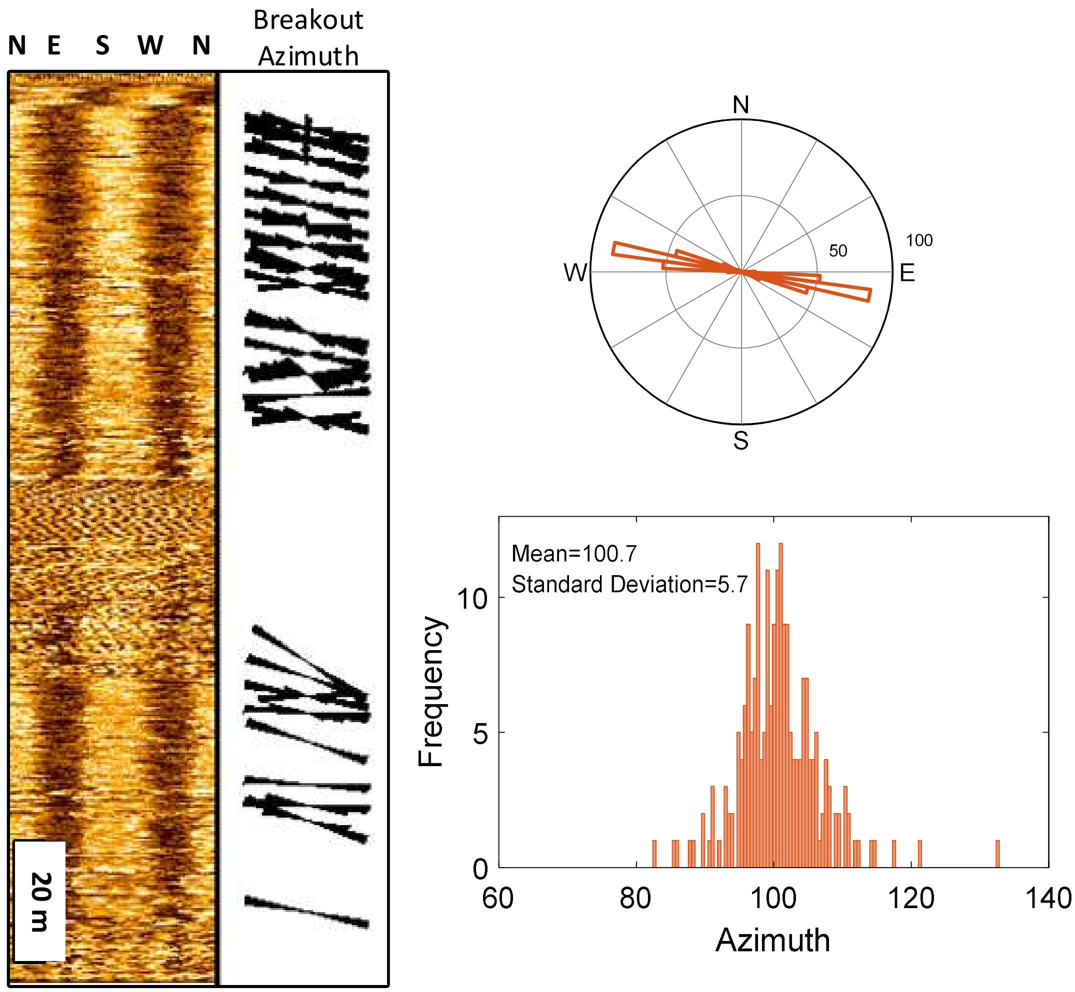

Figure 3: UBI log indicates that the minimum principal direction (borehole breakout) is 100°±5.7° in Well 7 of the West Paydar field.

Of all wells, wells CK-9, Lali-29, and the wells drilled in the Balarud field show signification variations and anomalies in breakout azimuths and tensile-induced fractures as a function of depth, due to stress perturbations associated with geological structures and faults. Figure S3 (supplementary materials) shows how breakout azimuths on the ultrasonic image logs for wells CK-9 and Lali-29 change abruptly at different depths, resume at slightly greater depths, and gradually change in the vicinity of the fault. Seismic interpretation (3D) results of the Cheshmeh-khosh field revealed two sets of faults with a NW-SE and WNW-ESE trend in the field, one of them close to well CK-9 (internal communication with NIOC). Talebi et al. (2018) and Hosseini et al. (2015) also observed that the stress orientations in the Lali field varied from well to well and were too complex to interpret due to an east-west trending strike-slip fault in the Asmari Formation. The Balarud Field is also a fault-bend fold where stress orientations are significantly affected and perturbed by their geological setting. The stress orientations in the western and eastern parts of the Balarud Field differ from each other and are highly variable.

Table 1: S_{Hmax} orientations by quality ranking derived from both borehole breakout (BO) and drilling induced fracture (DIF) in the different fields in the DE.

Field	Well Name abbreviation	Latitude	Longitude	S_{Hmax} Azimuth (deg)	Type	Number	Total length (m)	Depth (m)	Orientation (deg.)	S.D.	WSM (quality)
Aghajari	AJ-215	30.69	43.86	32	BO	5	110	2475	122	7.3	C
Balarud	BL-2	32.8	48.25	147.6	BO	6	140	2243	57.6	2.1	B
	BL-2	32.8	48.25	152.5	DIF	6	464	2174	152.5	11.1	B
	BL-3	32.78	48.36	175	BO	1	---	1616	85	----	D
	BL-3	32.78	48.36	174.9	DIF	10	269	1805	174.9	20	B
	BL-4	32.83	48.28	42.9	BO	19	503	1846	132.92	19.9	B
	BL-4	32.83	48.28	109.9	DIF	3	18	1705	109.9	18.6	D
	BL-6	32.71	48.31	169.08	DIF	24	623	1934	169.08	12.9	A
Bibi-Hakimih	BH-177	29.95	50.85	87.2	BO	51	210	1972	177.2	11.6	A
	BH-179	30.18	50.38	90.3	BO	109	520	2121	180.3	10.8	A
Chahar Bisheh	CB-4	29.88	51.12	52	BO	149	295	1953	142.0	9.9	A
Cheshmeh-khosh	CK-8	32.24	48.00	176	BO	25	238	3548	86.00	4.2	A
	CK-9	32.34	47.71	75	BO	43	221	4172	165.00	26.0	C
	CK-22	32.20	48.30	182.6	BO	10	106	3522	92.6	6.9	A
Dalpari	DP-08	32.54	47.83	157.3	BO	30	150	2340	67.3	32.1	D
Dehloran	DH-23	32.53	47.1	31.4	BO	52	415	4164	121.4	7.14	A
Khesht	KH-2	29.51	51.41	138	BO	28	402	2810	48.0	9.8	A
	KH-2	29.51	51.41	142.75	DIF	4	191	2845	322.75	8.7	C
	KH-5	29.44	51.29	124.05	BO	36	197	2994	34.05	8.7	A
	KH-5	29.44	51.52	119.4	DIF	19	215	2984	299.4	17.8	B
Lali	LL-22	32.25	134.2	44.2	BO	35	230	2278	44.2	11.2	A
	LL-29	32.22	48.11	135	BO	158	466	2547	46.10	43.3	E
Mansouri	MI-99	30.92	48.85	72.02	BO	22	179	3259	162.02	5.02	A
Maroun	MN446	31.524	49.324	75.7	BO	167	125	4293	165.70	5.3	A
Naft_Sefied	NS-47	31.60	49.31	72.75	BO	29	270	1625	162.75	9.78	A
Paydar	P-2	32.11	47.73	1.3	BO	89	681	3304	91.30	6.8	A
	P-2	32.11	47.73	179.2	DIF	99	576	3294	179.2	20.3	A
	P-6	32.14	47.54	10.7	BO	213	310	4045	100.7	5.7	A
	P-7	32.12	47.56	9.8	BO	135	230	4035	99.8	6.2	A
Ramshir	RR-19	30.65	49.6	59.65	BO	32	248	3061	149.65	6.70	A
	RR-19	30.65	49.6	70.8	DIF	3	48	2818	70.8	3.9	D
Yaran	YRRN-2	31.25	47.69	43.6	BO	11	140	3980	133.60	7.5	A

5.3 Stress Magnitude

Sufficient rock mechanics studies are available for the Sarvak and Asmari Formations to use in establishing the relation between static and dynamic elastic moduli and rock mechanics properties. The study carried out by Najibi et al. (2015) shows that the uniaxial compressive rock strength (UCS) of limestone in the Sarvak and Asmari Formation varies considerably between 30 to 180 MPa, with the most frequent value being 80 MPa (Figure 4.b). The same results have been reported by other studies (Asadi et al., 2013; Asef and Farrokhrouz, 2010; Cheshomia and Ahmadi, 2013; Farrokhrouz et al., 2014; Haghnejad et al., 2014; Haghnejad et al., 2013; Koleini, 2012; Mazidi Saber Mehrabi et al., 2012; Najibi and Asef, 2014; Najibi et al., 2015). Note that the Asmari and Sarvak Formations, as described above, also contain sandstone and shale of lower strength than the carbonate parts.

To 7 km depth, three abnormally pressured formations are present in the DE: the Miocene evaporitic Gachsaran Formation (Lower Fars), the Triassic Dashtak Formation and the Lower Cretaceous carbonate Fahliyan Formation. Almost all wells drilled in the Embayment experience difficulties in penetrating the Gachsaran Formation, sometimes leading to blowouts (Nabaei et al., 2011). The pressure gradient in the Gachsaran Formation ranges from 15.5 to 22.1 MPa/km in several oil fields located in the DE such as Masjid-i-Sulaiman, Lali, Haft-Kel, Naft Safid, AghaJari, Pazanan, Gachsaran, and Naft Shahar. The Dashtak Formation in the Embayment is located at a greater depth. The pressure variation along the Triassic Dashtak Formation is equivalent to that of the Gachsaran formation due to both having evaporitic rock composites; however, the former is the caprock in the Fars region hydrocarbon fields. Drilling experience in the Fars region shows that high mud weights are needed to drill into the Dashtak Formation (Salehi et al., 2012). The lower Fahliyan Formation, which mainly consists of limestone, is another location of slight overpressure in the ZFTB, mostly in the Abadan plain province (Atashbari, 2016; Soleimani et al., 2017). Figure S2 of the supplementary materials shows variations of mud weight and direct pore pressures with depth from observations of several wells in the DE.

Figure 4.a illustrates the required rock strength (UCS) for a case S_v = 78 MPa, S_{Hmax} = 72 MPa, S_{hmin} = 37 MPa, and P_p = 30 MPa. The Mohr–Coulomb failure criterion and Kirsch formulation (equation (2)) (Jaeger et al., 2009) were used in these calculations. The presence of breakouts provides a lower bound on the stress difference, whereas its absence places an

upper bound on the stress anisotropy around the borehole. Considering these bounds and applying the above equation based on Anderson's faulting theory (equation (1) , and assuming the state of stress is in frictional failure equilibrium, Figure 4 illustrates two possible states of stress, extensional (normal/strike-slip) (Figure 4.c) and compressional (reverse/strike-slip) (Figure 4.d), in the sedimentary cover of the DE (see Figure 9 Moos and Zoback (1990) for more information). A depth between 3000 to 4500 m has been chosen since the reservoir formations, the Asmari and Sarvak in the DE, are generally located at such depths, and most of the relevant conventional petrophysics logs are usually available. The color in Figure 4 shows the effective rock strength needed to prevent breakouts, or the value below which compressive failure occurs. In each case, S_v is assumed to be a principal stress and is equal to the weight of the overburden rocks ($\rho \approx 2.6$ g/cm^3).

It is clear that in a compressional stress system in the studied region, the minimum effective rock strength to prevent borehole failure should be more than 250 MPa. Hence, considering the average UCS value of 100 MPa in the Sarvak and Asmari Formations, one would expect to observe continuous breakouts at all azimuths around a drilled borehole at almost any depth. Therefore, S_{Hmax} must be less or close to S_v (a normal/strike-slip regime), and the required rock strength is expected to be around 100 MPa (Figure 4.a).

Many oil and gas wells have been drilled vertically into the Sarvak and Asmari Formations in the studied area, with no instability problems. Directional wells, however, do experience instability, and normally need more mud weight for safe drilling. Directional wells drilled in the direction of minimum principal stress (borehole breakout azimuth) are much more stable, as less stress anisotropy is acting around the borehole wall. For example, well-7 in the West Paydar Field is side-tracked in two azimuths of 212° and 292°: ST-1, the first side-track at azimuth 212°, was drilled 212 meters in 20 days with a mud weight of 70 pcf, and ST-2 was drilled 717 meters in 15 days at azimuth 292° with a mud weight of 63 pcf. This drilling experience example supports the counterintuitive fact that the state of stress in the sedimentary cover of the DE is a normal/strike-slip regime.

These results are similar to those reported by Yaghoubi and Zeinali (2009) in the Cheshmeh-khosh field and Haghi et al. (2018) in the Mansouri field in the southern part of the DE. Their results show that normal/strike-slip faulting predominates in the sedimentary cover to a depth of 5 km. Haghi et al. (2018) performed borehole geomechanics modelling of the Sarvak Formation in the southern part of the DE and determined through extended leak-off tests (XLOT) that the S_{hmin} gradient varies from 15.2 MPa/km (0.67 psi/ft) to 17.4 MPa/km (0.77 psi/ft). The normal/strike-slip faulting regime in the shallow sedimentary cover of the DE is also consistent with little seismicity and fault slip. A micro-earthquake study by (Yamini-Fard et al., 2006) revealed that the shallower sedimentary cover deforms by less compressive state of stress and confirms the legitimacy of our results.

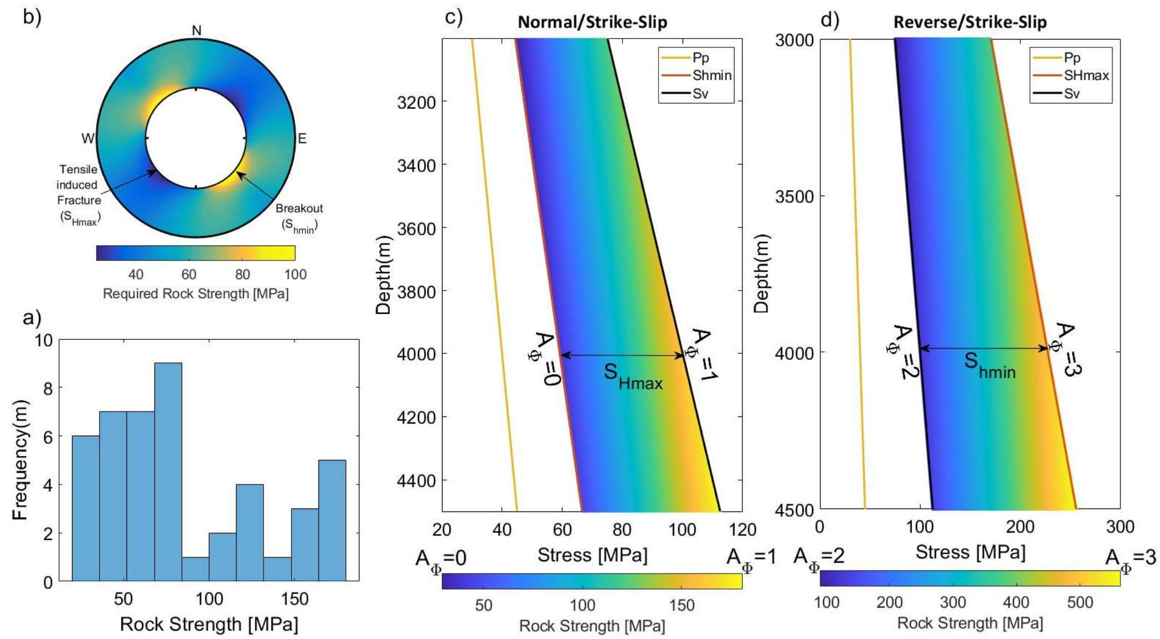

Figure 4: b) The uniaxial compressive rock strength (UCS) histogram of limestone in the Sarvak and Asmari Formations of the Mansori field; b) example of stress concentration around a vertical borehole and the location of borehole breakout and tensile induced fracture and their relation to principal stress orientations;. c) and d) rock strength required to initiate a breakout in normal and reverse faulting regimes in the Sarvak and Asmari Formations of the DE, assuming that the stresses at the limit are constrained by a friction coefficient $\mu = 0.6$, P_p = 10 MPa/km, and S_v = 26 MPa/km (equation (1)). The color bar shows rock strength needed to prevent borehole breakout in vertical boreholes. Mohr–Coulomb failure criterion and Kirsch equations (equation (2)) were used in these calculations.

6. State of the Stress from Earthquake Focal Mechanisms

More than 5000 earthquakes with $M_w \geq 3$ have been recorded in the area since 2010 (Iranian Seismological Centre). Their magnitude and distribution increase from northwest to southeast, but they are scattered and rarely associated with co-seismic surface rupture (except in the case reported by Walker et al. (2005)). Most have occurred on active blind and hidden faults (Berberian, 1995) beneath sedimentary cover (Figure 1). There is always uncertainty associated with pinpointing the depth of an earthquake; however, of the earthquakes observed in the ZFTB, most occurred deeper underground and fewer occurred at shallow depths in the sedimentary cover (histogram in Figure 1). Talebian and Jackson (2004) stated that rarely have earthquakes in the ZFTB been associated with surface faulting. Many other scientists have performed studies on the earthquake depths in the ZFTB and confirmed that the sedimentary cover is less seismically active even though it has been crisscrossed by many faults, as shown in Figure 1 (Hatzfeld et al., 2010; Lacombe et al., 2006; Molinaro et al., 2005; Tatar et al., 2004). Rarely have earthquakes with a Mw greater than 7 been recorded in the ZFTB.

In Figure 5, two NE-SW cross-sections of a) the northern (A-A′) and b) southern parts (B-B′) of the DE delineate topographic profiles accompanied by the location of earthquakes. As illustrated in Figure 1 inset and Figure 5, most of the earthquakes are located and nucleate at a depth greater than 5 km, and are confined between 10 and 15 km, below the sedimentary cover at the site of hidden faults. Seismic events are restricted to an elevation less than 1500 m in the area where most oil and gas fields are located (the embayment area).

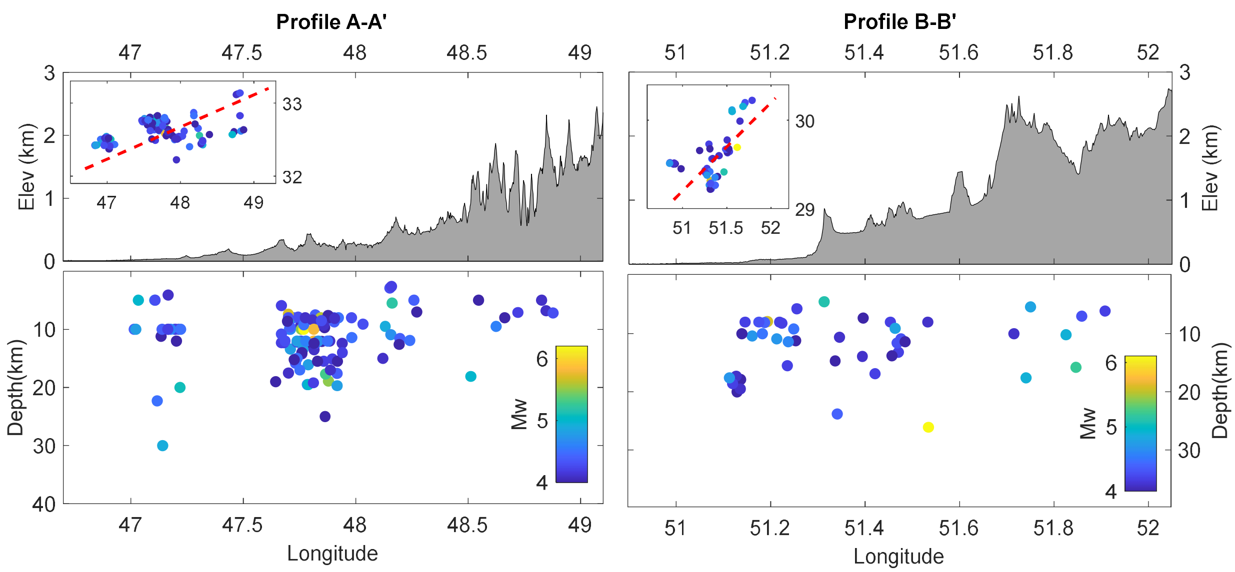

Figure 5: Cross-sections of DE displaying topography and seismicity in A-A′ and B-B′ sections shown in Figure 1. The colour scale represents earthquake magnitudes. The high seismicity density in the area is restricted to below 4 km. Details of each earthquake are provided in the supplementary materials (Table S2).

6.1 Methodology

Earthquake focal mechanisms allow the development of constraints on relative stress magnitudes. Assuming that S_v is one of the principal stresses, an appropriate stress regime for each earthquake focal mechanism can be assigned based on WSM criteria (Table 3, Zoback (1992)). The S_{Hmax} orientation can also be determined from single earthquake focal mechanism (FMS) and the formal stress inversion of those focal mechanisms (FMF). Whereas the FMS are only approximate indicators of S_{Hmax} orientation, the inversion of sets of earthquake focal mechanisms determines a best-fitting stress field and provides a more accurate estimation of the principal stress orientations (Gephart and Forsyth, 1984; Michael, 1984). In this study, we conduct a formal inversion of moment tensors using MSATSI Matlab code which iteratively inverts for the stress field based on SATSI algorithm (Lund and Townend, 2007; Martínez-Garzón et al., 2014). Assuming also that stress magnitudes at each depth are consistent with Coulomb frictional-failure theory for a coefficient of friction, Angelier (1984) introduced a quantity ϕ, defined by the equation

$$\varphi = S_2 - S_3/S_1 - S_2 \quad (3)$$

where S_1, S_2, and S_3 are the maximum, intermediate, and minimum principal stresses. Depending on the magnitude of the intermediate stress relative to the other two, Angelier's shape parameter ϕ must fall between zero and one (Hurd and Zoback, 2012). Otherwise, none of the nodal planes will be geometrically consistent. Once the stress tensor is known, ϕ values and error limits can be computed at the same time as the principal stresses and axes. Simpson (1997) generalized the parameter ϕ values to provide a quantitative measure as an equation:

$$A_\phi = (n + 0.5) + (-1)^n(\phi - 0.5) \quad (4)$$

where n=0, 1, 2, for normal, strike-slip and reverse types of faulting respectively. The Anderson fault parameter A_ϕ (The style of faulting) ranges continuously from 0 to 1 for normal, 1 to 2 for strike-slip, and 2 to 3 for reverse faults (Yang and Hauksson, 2013).

6.2 Stress Orientation

The S_{Hmax} orientation has been determined from 108 single earthquake focal mechanisms and the formal stress inversion of those focal mechanisms (Table S2 in the supporting material). The total data cluster into three groups based on their location (latitude and longitude), so stress inversion is calculated for each group using the method presented in Martínez-Garzón et al. (2014) (see Figures S4 and S5 for more information). Table 2 contains the results of the formal stress inversion. The red lines crossing the beachballs in Figure 6 show the 108 S_{Hmax} orientations inferred from individual focal mechanisms (P-axis), while the inward-pointing black arrows (reverse faulting regime) and green arrows (strike-slip) represent the S_{Hmax} direction calculated from formal stress inversion in the DE.

Seismologically determined maximum horizontal stress (S_{Hmax}) orientations show more overall consistency and spatial uniformity than those obtained from the borehole wall examination (the blue lines with inward pointing arrows in Figure 7). The study suggests that the evaluated earthquakes are in both a thrust and a strike-slip faulting regime, with an average S_{Hmax} orientation of 37°±10°. However, stress orientation variations are seen in most of the investigated oil and gas fields, from relatively abrupt changes of borehole breakout orientation when drilling crosses a fault, to gradual variations over scales of several hundred meters. The resultant spatial variation of stress orientations in different locations of the study area shows general stress heterogeneity (discussed later).

Table 2: Stress inversion results at different locations in the DE.

Lat (°N)	Long (°W)	Number of Focal Mechanisms	S1 Azimuth (°)	S1 Plunge (°)	R=(1-φ)	Faulting Regime
48	33	68	205	4.1	0.72±0.2	R
52	29	31	223	5.7	0.78±0.25	R
51.6	29.8	23	221	4.3	0.84±0.15	S

6.3 Relative Stress Magnitudes and Style of Faulting

Employing Simpson's (1997) approach, Figure 6 displays the results of focal mechanisms analysis and the fault-type regimes on each focal mechanism. The color inside of each focal beachball indicates the style of faulting based on A_ϕ values. Noticeably, the highest frequency value for $A_\phi \cong 2.2$, suggesting that S_{Hmax} is considerably greater than the vertical stress (S_3) and S_{hmin} (S_2) and S_{hmin}/S_V stress permutations. This compressional environment regime corresponds to a state in which both the reverse fault and strike-slip fault are potentially active. Of the 108 earthquake focal mechanisms considered, 22 earthquakes occurred in response to a strike-slip stress state at various locations, but most occurred around the NS striking Kazerun Fault.

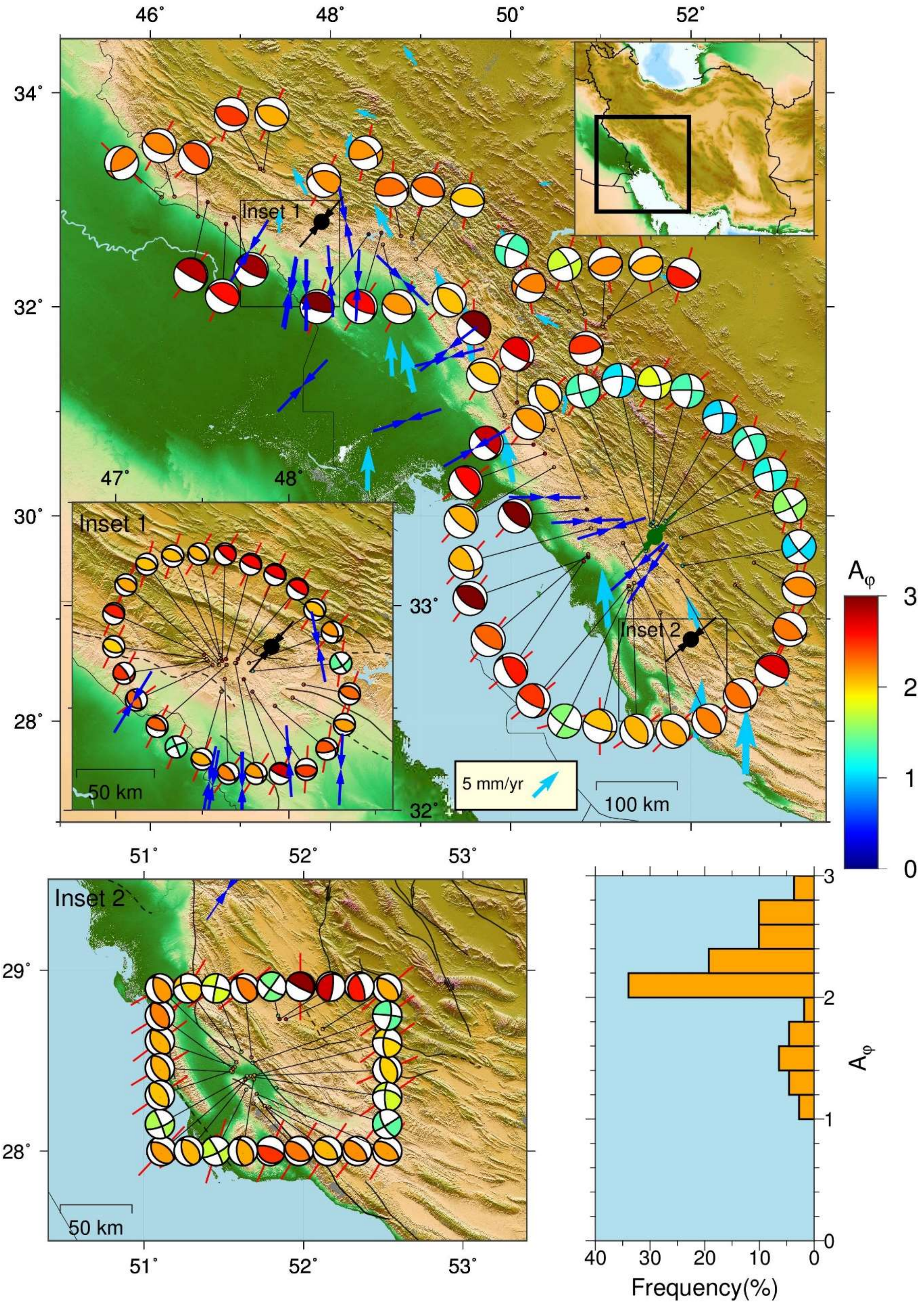

Figure 6: Map view of the value of 108 interpreted focal mechanisms in the Dezful Embayment. Colors show the stress regimes, with A_ϕ value ranging 0.0 to 1.0 for normal faulting, 1.0 to 2.0 for strike-slip faulting, 2.0 to 3.0 for reverse faulting. Red and black lines indicate the orientation of S_{Hmax} for

individual focal earthquakes (P-Axis) and formal stress inversion respectively. Blue inward arrows show the S_{Hmax} direction derived from borehole breakouts and induced tensile fractures of A quality (Table 1). The light blue arrow is GPS velocity vectors relative to central Iran derived from Walpersdorf et al. (2006). The greatest concentration of earthquakes is around the Balarud fault in the northern part of the embayment (inset 1).

7. Seismicity and fault slip compatibility

The occurrence of fewer earthquakes in an area can generally be explained in two ways. First, the state of stress in an area is not sufficient to exceed the rock's frictional strength to the point that a failure/earthquake is nucleated by the relative stress magnitudes (Snee and Zoback, 2016). Second, there may be no permeable, critically stressed faults in the area with respect to in-situ stress orientation (Snee and Zoback, 2016). Hence, the presence or absence of seismicity with respect to fault orientations in an area with known stress orientation will provide information on the stress magnitudes. This section first investigates which of two nodal planes for an earthquake focal mechanism is geometrically optimal for fault slip, and what the frictional likelihood is of a slip occurring along the preferred nodal plane. Then, the relationship between seismicity and the state of stress is investigated, particularly in the Kazerun Fault area.

Slip along a fault depends on the relative stress magnitude and the angle between the principal stress directions and the fault plane, plus the coefficient of friction μ (Morris et al., 1996). The slip tendency on a pre-existing cohesionless fault can be defined in terms of the Mohr-Coulomb shear failure criteria

$$\mathrm{CFF} = \tau - \mu\sigma_n \quad (5)$$

where τ and σ_n are shear and effective normal stress acting on a pre-existing fault plane, and μ is the coefficient of friction. Slip is likely to occur on a fault plane when the resolved shear stress, τ, equals or exceeds the frictional resistance of the fault's surface ($\tau \geq \sigma_n\mu$), and in which case the fault is called critically stressed.

Earthquakes in the Zagros area occur along blind/hidden faults for which neither geological mapping nor 3D seismic imaging can clearly determine the geometries (Berberian, 1995). However, existing faults can now be inferred from induced seismic events. Using earthquake focal mechanisms that provides two nodal planes, we can deduce the possible fault plane. Figure 7.a illustrates a normalized 3D Mohr diagram with a representative reverse focal event (M_w=4.2, 2015-08-14). The stress magnitude in the diagram is based on the A_ϕ value calculated for the event. The circle points in Figure 7.a correspond to the normalized shear and normal stress acting on each nodal plane. As shown for this example, the plane fault striking NW-SE and dipping $30°$ NE is most likely to slip and is the preferred nodal plane. Figure 7.b shows the slip-tendency in a case where the state of stress is the reverse faulting regime ($A_\phi = 2.2$), with an average S_{Hmax} orientation of N20°E and hydrostatic pore pressure. Red represents critically stressed fault poles and blue corresponds to fault poles with a lower likelihood of slip (τ/σ_n). Small-circles on the stereonet represent 92 preferentially-oriented nodal planes. The result shows that in the reverse fault regime, where S_{Hmax} is oriented NEE, faults striking NW-SE and dipping $40° - 60°$ either NE or SW are most likely to slip. According to the analysis, a sliding friction coefficient of 0.5–0.6 can be inferred as an optimum friction angle for NW-SE oriented faults in the Zagros.

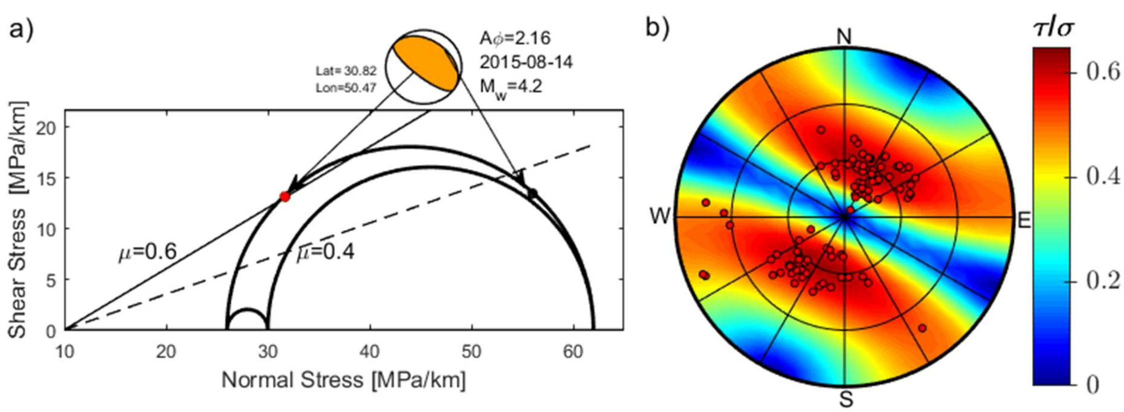

Figure 7: a) 3D Mohr's circle showing representative reverse focal plane mechanisms and resolved shear and normal stresses for each nodal plane. The color inside the beach ball represents A_ϕ and is based on the color bar shown in Figure 6. b) Lower hemisphere stereonet plot of the preferred nodal plane for 92 focal plane mechanisms in the DE where the state of stress is a thrust-faulting regime. Colors show the ratio of shear to effective normal stresses (required μ) needed for shear failure on a fault plane.

Despite relatively uniform compressive stress orientations on both sides of the N-S Kazerun transverse active fault, the relative principal stress magnitudes inferred from earthquake focal mechanisms abruptly changed from a reverse faulting regime to a pure strike-slip faulting regime near the fault segment (Figure 8). Previous studies (Baker et al., 1993; Maggi et al., 2000; Talebian and Jackson, 2004) have stated that the strike-slip fault along the old inherited basement Kazerun fault occurred at a depth of 4-10 km, with an average depth uncertainty ±3 in the sedimentary cover, and in the uppermost basement. In contrast, reverse-faulting focal mechanisms occurred at greater depths in the basement. In fact, the state of stress in the different sides of the Kazerun faulting zone does not change laterally but rather vertically. The same results were reported after seven weeks' observations of micro-seismicity around the northern end of the near-vertical Kazerun fault, in which slips at greater depths occurred in response to a pure reverse faulting regime (Yamini-Fard et al., 2006). Nearly all of the shallow-depth events resulted from a pure strike-slip regime.

This finding aligns with the frictional faulting theory that the N-S trending Kazerun fault is in an unfavorable orientation for slip in a reverse fault regime with an average SW-NE S_{Hmax} orientation. In Figure 8.c, black circles on the stereonet plot represent the seismologically actual fault plane around the Kazerun fault systems showing that the N-S strike fault has a higher slip likelihood. The same fault plane in a reverse faulting regime is not in a geometric state permitting nucleation of an earthquake, except for a fault surface having the frictional strength within $\mu \approx 0.3$-0.4. In fact, because the state of stress varies with depth, the slipping tendency for a N-S strike fault increases when the state of stress changes to the strike-slip regime at the upper depths.

High heat flow in fault zones generally indicates a fault's frictional resistance to slip and implies that the fault is frictionally strong. Heat flow measured in different oil and gas wells in the DE reflects significantly higher temperatures in the vicinity of the Kazerun fault (66 mW/m^2) (Figure 4 Rudkiewicz et al. (2007)), whereas the central and northern embayment has a mean heat flux between 30-40 mW/m^2. No particular reason is stated for such a high thermal anomaly around the Kazerun line, but one can assume that it results from friction and that fault is not weak. This supposition is consistent with lack of reverse slip around the fault, as the frictional strength needs to be as low as 0.3-0.4 and explains why most earthquakes around the Kazerun fault are a response to a strike-slip stress state. Note that the reverse slip observed in the northern Kazerun fault system is small in magnitude (Yamini-Fard et al., 2006).

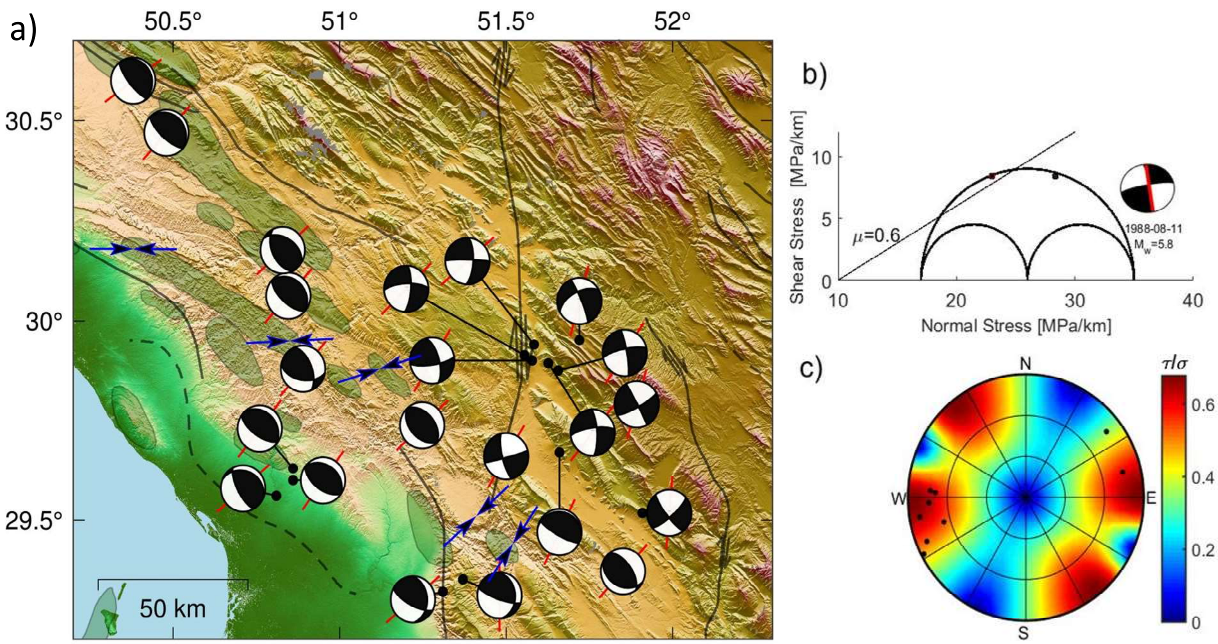

Figure 8: a) Earthquake focal mechanisms in the vicinity of the N-S Kazerun transverse active fault. The state of stress changes from strike-slip faulting around the fault to a reverse faulting regime on either side whereas the seismologically (red line) determined azimuth S_{Hmax} (P-Axis) is stable and uniform around the area. b) 3D Mohr's circle showing a representative strike-slip focal plane mechanism and resolved shear and normal stresses for each nodal plane. The red line on the focal beach-ball indicates the actual fault plane. c) Lower hemisphere stereonet plot illustrates the slip-tendency (ratio of resolved shear to normal stress) associated with the strike-slip Kazerun fault and actual nodal plane for 12 focal plane mechanisms mapped in (a).

8. Discussion

The stress orientation in the sedimentary rock strata and in the basement shows two entirely distinct types. The stress orientations constrained from inversion of the focal mechanisms consistently run in the NE-SW direction in all areas of the ZFTB. However, variations of stress orientations (blue arrow line in Figure 6) are seen in most of the investigated oil and gas fields in the area, from relatively abrupt changes of borehole breakouts to gradual variations over scales of several hundred meters.

Stress deflection or second-order stress pattern can be due to lateral density/strength contrasts, flexural stresses or superimposed geological structures such as faults (Sonder, 1990). The magnitude of local stresses relative to regional stress along with the angle between local structures and the regional stress orientation are all significant parameters in measuring the deviation of local stress orientation (Sonder, 1990; Zoback, 1992).

The regional horizontal stress difference (S_{Hmax}-S_{hmin}) is the determining factor (Sonder, 1990) for these anomalies in the folded and faulted sedimentary cover in the ZFTB. With this compressional state of the stress field at seismogenic depths (7-15 km) in the ZFTB, where S_{Hmax}-$S_{hmin} \approx 30$ MP, the local uniaxial stress is not sufficient to deflect stress orientation. However, in the sedimentary rock where the regional state of stress has been constrained to be on the border between normal and the strike-slip faulting regime ($\mathrm{S_{Hmax}} \cong \mathrm{S_V} > \mathrm{S_{hmin}}$), a moderate local horizontal stress difference can cause stress deflection. Thus, variations in stress orientations are seen in most of the oil and gas fields examined in the DE.

Stress variation with depth can be explained by decoupling of the stress because of the existence of a ductile formation (Ahlers et al., 2019; Cornet and Röckel, 2012; Roth and Fleckenstein, 2001). The ZFTB can be considered as a classic case for stress decoupling and varying stress regime with depth in sedimentary basins due to several continuous highly ductile formations: Precambrian Hormuz, Triassic Dashtak, and Miocene Gachsaran Formations. These formations can shield the shallower sediments from the compressional strains in the basement rock arising from the collision between the Arabian and Eurasian plates (Bahroudi and Koyi, 2003; Molinaro et al., 2005; Sepehr and Cosgrove, 2004; Walpersdorf et al., 2006). These detachment horizons also can result in decoupling of the basement and overburden deformation during the crustal compression. Such vertical variation in the state of stress regime has been observed in the eastern part of the Paris Basin (Cornet and Röckel, 2012), the eastern North German Basin (NGB) (Ahlers et al., 2019; Roth and Fleckenstein, 2001), and the Nile Delta (Tingay et al., 2011).

Fewer earthquakes in an area can generally be explained by a state of stress in a faulted area that is not sufficient to exceed the rock's frictional strength to the point that an earthquake is nucleated by the relative stress magnitudes. This phenomenon could explain the situation in DE. Both regional geophysics and geological studies of the DE have revealed its sedimentary cover to be crisscrossed by faults at both low and highly elevated areas. Similarly, many oil and gas boreholes have been drilled through local faults (Figure 3S); nevertheless, earthquakes in the sedimentary cover are rare.

Since most faults in the area strike NW-SE, almost perpendicular to the maximum horizontal stress orientation, they are critically stressed and associated with seismicity only in the reverse faulting regime (Figure 7). Consequently, the state of stress in the sedimentary cover cannot be as strongly compressional as the basement; otherwise, more earthquakes would be expected in the area. In fact, the few earthquakes occurring at shallow depths compared to the number at greater depths in the area, plus the present NW-SE striking faults, strongly indicate that the state of stress in the sedimentary cover in all areas of the DE is a normal/strike-slip faulting regime. This fact confirms that the state of stress in the sedimentary cover is gradually changing from extensional to compressional from the sedimentary cover to the basement.

Figure 9 shows fault stability analysis of faults mapped in the Zagros area color-coded by CFF; it is assumed that $\mu = 0.5$, and the state of stress is on the border of the strike-slip and normal faulting regimes ($S_{Hmax} \cong S_V > S_{hmin}$), as illustrated in the lower left inset in the 3D Mohr diagram. The positive CFF indicates that the shear stress on the fault plane exceeds the effective normal stress ($\tau \leq \mu\sigma_n$), meaning that slip occurs along the failure plane and the fault is unstable. In a normal faulting regime with an average S_{Hmax} orientation of $N025°E$, the NW striking faults will have highly unfavourable orientations for the slip. The locations of earthquakes since 2009 at a depth above 6 km are mapped as black circles in Figure 9. These earthquakes are scattered over the area, except for the August 2014, Murmuri Mw 6.2 event in the north of the DE. The analysis has determined that earthquakes are concentrated within the basement and concludes that the state of stress at the near-surface deposits is not as compressional as that deeper in the basement.

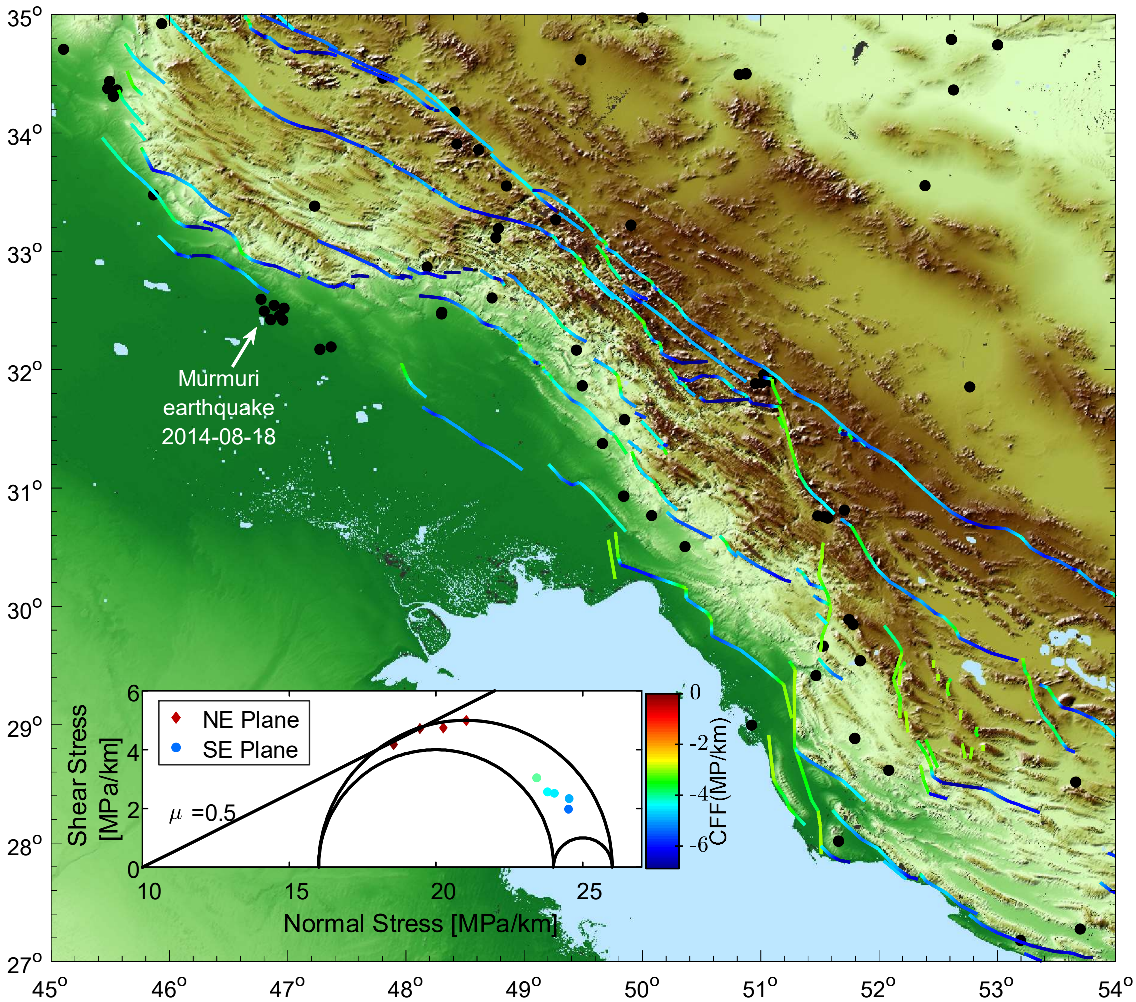

Figure 9: Large-scale faults examined in slip tendency analysis, in terms of CFF for normal state of stress in sedimentary cover of DE. The CFF ($\tau - \mu\sigma_n$) colour value is normalized with depth. Black circles represent earthquakes at a depth above 6 km with Mw=>4 in the area since 2010. The lower left inset illustrates 3D Mohr diagram frictional slip stability assigned for the slip tendency analysis.

9. Conclusions

The state of stress and the style of faulting for the DE in the ZFTB was investigated using data from boreholes drilled for hydrocarbon resources development and from earthquake focal plane mechanism records. The study supports the following findings:

1. Geomechanics study on 25 boreholes confirms that the stresses in the sedimentary cover are less compressional at shallow depths (i.e., normal and strike-slip faulting). This finding is consistent with fault slip tendency analysis of the sedimentary cover, and the fewer earthquakes at shallower depths, as well as the leak-off test results reported by other researchers.

2. The style of faulting and relative stress magnitudes and stress orientation in the area were investigated using Simpson's (1997) approach in 108 well-constrained earthquake focal plane mechanisms. This analysis shows that the Anderson fault parameter, A_{ϕ}, varies from 2 (strike-slip faulting) to 3 (reverse faulting) in the DE, with the highest frequency being between 2.0-2.2, suggesting that the style of faulting in the basement is compressional (a reverse to strike-slip faulting regime) because the S_{Hmax} and S_V magnitudes are close to one another, but far higher than the minimum horizontal stress value.
3. Studying both the sedimentary cover and the basement of the DE shows a change from the normal/strike-slip faulting stress regime in the former to a thrust–fault stress regime in the latter.
4. Critically stressed fault analysis using the Mohr-Coulomb failure criterion was applied to both the sedimentary cover and the basement in the DE. The analysis shows that the most-likely fault plane to slip in the basement is a high angle fault (75°-80°) aligned NW-SE. The local shallow depth faults, mostly lying NW-SE, are not critically stressed, and in fact, at the current state of stress, they are mechanically quiescent. This observation is consistent with the very few earthquakes occurring in the upper part of the sedimentary cover of the DE.

Acknowledgments

We would like to thank Shahram Sherkati and Mojtab Rajabi for comments on preliminary version of the paper. The Generic Mapping Tools (GMT) (Wessel and Smith, 1998) was used to generate some figures. All earthquake data used in this study are openly available from Iranian Seismological Centre (www.irsc.ut.ac.ir) or in the supplementary materials.

Reference

Adams, A., Brazier, R., Nyblade, A., Rodgers, A., Al-Amri, A., 2009. Source parameters for moderate earthquakes in the Zagros Mountains with implications for the depth extent of seismicity. Bulletin of the Seismological Society of America 99, 2044-2049.

Agard, P., Omrani, J., Jolivet, L., Mouthereau, F., 2005. Convergence history across Zagros (Iran): constraints from collisional and earlier deformation. International journal of earth sciences 94, 401-419.

Ahlers, S., Hergert, T., Henk, A., 2019. Numerical Modelling of Salt-Related Stress Decoupling in Sedimentary Basins–Motivated by Observational Data from the North German Basin. Geosciences 9, 19.

Alavi, M., 1994. Tectonics of the Zagros orogenic belt of Iran: new data and interpretations. Tectonophysics 229, 211-238.

Alavi, M., 2004. Regional stratigraphy of the Zagros fold-thrust belt of Iran and its proforeland evolution. American journal of Science 304, 1-20.

Alavi, M., 2007. Structures of the Zagros fold-thrust belt in Iran. American Journal of science 307, 1064-1095.

Allen, M., Saville, C., Blanc, E., Talebian, M., Nissen, E., 2013. Orogenic plateau growth: Expansion of the Turkish-Iranian Plateau across the Zagros fold-and-thrust belt. Tectonics 32, 171-190.

Allen, M.B., Talebian, M., 2011. Structural variation along the Zagros and the nature of the Dezful Embayment. Geological Magazine 148, 911-924.

Angelier, J., 1984. Tectonic analysis of fault slip data sets. Journal of Geophysical Research: Solid Earth 89, 5835-5848.

Asadi, S., Maleki, J.M., Bohloli, B., Mutabashiani, S., 2013. Experimental, Numerical and Analytical Investigation the Initiation and Propagation of Hydraulic Fracturing. World Applied Sciences Journal 22, 637-646.

Asef, M.R., Farrokhrouz, M., 2010. Governing parameters for approximation of carbonates UCS. Electron.J.Geotech.Eng 15, 1581–1592.

Atashbari, V., 2016. Origin of overpressure and pore pressure prediction in carbonate reservoirs of the Abadan Plain Basin, Australian School of Petroleum. University of Adelaide.

Bahroudi, A., Koyi, H.A., 2003. Effect of spatial distribution of Hormuz salt on deformation style in the Zagros fold and thrust belt: an analogue modelling approach. Journal of the Geological Society 160, 719-733.

Bahroudi, A., Koyi, H.A., 2004. Tectono-sedimentary framework of the Gachsaran Formation in the Zagros foreland basin. Marine and Petroleum Geology 21, 1295-1310.

Baker, C., Jackson, J., Priestley, K., 1993. Earthquakes on the Kazerun Line in the Zagros Mountains of Iran: strike-slip faulting within a fold-and-thrust belt. Geophysical Journal International 115, 41-61.

Bell, J.S., Gough, D.I., 1979. Northeast-southwest compressive stress in Alberta: evidence from oil wells. Earth Planet Sci Lett 475–482.

Berberian, M., 1995. Master “blind” thrust faults hidden under the Zagros folds: active basement tectonics and surface morphotectonics. Tectonophysics 241, 193-224.

Bordenave, M.L., Burwood, R., 1995. The Albian Kazhdumi Formation of the Dezful Embayment, Iran: One of the Most Efficient Petroleum Generating Systems, in: Katz, B.J. (Ed.), Petroleum Source Rocks. Springer Berlin Heidelberg, Berlin, Heidelberg, pp. 183-207.

Bordenave, M.L., Hegre, J.A., 2010. Current distribution of oil and gas fields in the Zagros Fold Belt of Iran and contiguous offshore as the result of the petroleum systems. Geological Society, London, Special Publications 330, 291-353.

Cheshomia, A., Ahmadi, S., 2013. Determination of uniaxial compressive strength of microcrystalline limestone using single particles load test. Journal of Petroleum Science and Engineering 111, 121-126.

Cornet, F.H., Röckel, T., 2012. Vertical stress profiles and the significance of "stress decoupling". Tectonophysics 581, 193-205.

Dusseault, M.B., 2011. Geomechanical challenges in petroleum reservoir exploitation. KSCE Journal of Civil Engineering 15, 669-678.

Dusseault, M.B., Bruno, M.S., Barrera, J., 1998. Casing shear: causes, cases, cures, SPE International Oil and Gas Conference and Exhibition in China. Society of Petroleum Engineers.

Fakhari, M.D., Axen, G.J., Horton, B.K., Hassanzadeh, J., Amini, A., 2008. Revised age of proximal deposits in the Zagros foreland basin and implications for Cenozoic evolution of the High Zagros. Tectonophysics 451, 170-185.

Farrokhrouz, M., Asef, M.R., Kharrat, R., 2014. Empirical estimation of uniaxial compressive strength of shale formations. GEOPHYSICS 79, D227–D233.

Gephart, J.W., Forsyth, D.W., 1984. An improved method for determining the regional stress tensor using earthquake focal mechanism data: application to the San Fernando earthquake sequence. Journal of Geophysical Research: Solid Earth 89, 9305-9320.

Haghi, A., Chalaturnyk, R., Ghobadi, H., 2018. The state of stress in SW Iran and implications for hydraulic fracturing of a naturally fractured carbonate reservoir. International Journal of Rock Mechanics and Mining Sciences 105, 28-43.

Haghnejad , A., Ahangari, K., Ali, N., 2014. Investigation on Various Relations Between Uniaxial Compressive Strength, Elasticity and Deformation Modulus of Asmari Formation in Iran. Arab J Sci Eng 39, 2677–2682.

Haghnejad, A., Ahangari, K., Noorzad, A., Minaeian, B., 2013. Prediction Relations between Physical and Mechanical Properties of Rocks: A Case Study of Asmari Formation in Iran. International Journal of Geosciences Research 1, 1-8.

Hatzfeld, D., Authemayou, C., Van Der Beek, P., Bellier, O., Lavé, J., Oveisi, B., Tatar, M., Tavakoli, F., Walpersdorf, A., Yamini-Fard, F., 2010. The kinematics of the Zagros mountains (Iran). Geological Society, London, Special Publications 330, 19-42.

Hauksson, E., 1994. State of stress from focal mechanisms before and after the 1992 Landers earthquake sequence. Bulletin of the Seismological Society of America 84, 917-934.

Heidbach, O., Rajabi, M., Reiter, K., Ziegler, M., 2016. World stress map 2016. Science 277, 1956-1962.

Heidbach, O., Tingay, M., Barth, A., Reinecker, J., Kurfeß, D., Müller, B., 2010. Global crustal stress pattern based on the World Stress Map database release 2008. Tectonophysics 482, 3-15.

Hosseini, E., Ghojogh, J.N., Habibnia, B., 2015. Study of Faults in Asmari Formation by FMI Image Log, Case Study: Lali Oilfield. American Journal of Oil and Chemical Technologies: Volume 3.

Hosseini, H., Pakzad, M., Naserieh, S., 2019. Iranian regional centroid moment tensor catalog: solutions for 2012–2017. Physics of the Earth and Planetary Interiors 286, 29-41.

Hurd, O., Zoback, M.D., 2012. Intraplate earthquakes, regional stress and fault mechanics in the Central and Eastern US and Southeastern Canada. Tectonophysics 581, 182-192.

Jackson, J., Fitch, T., 1981. Basement faulting and the focal depths of the larger earthquakes in the Zagros mountains (Iran). Geophysical Journal International 64, 561-586.

Jackson, J., McKenzie, D., 1984. Active tectonics of the Alpine—Himalayan Belt between western Turkey and Pakistan. Geophysical Journal International 77, 185-264.

Jaeger, J.C., Cook, N.G., Zimmerman, R., 2009. Fundamentals of rock mechanics. John Wiley & Sons.

Jahani, S., Callot, J.-P., de Lamotte, D.F., Letouzey, J., Leturmy, P., 2007. The Salt Diapirs of the Eastern Fars Province (Zagros, Iran): A Brief Outline of their Past and Present, in: Lacombe, O., Roure, F., Lavé, J., Vergés, J. (Eds.), Thrust Belts and Foreland Basins: From Fold Kinematics to Hydrocarbon Systems. Springer Berlin Heidelberg, Berlin, Heidelberg, pp. 289-308.

James, G., Wynd, J., 1965. Stratigraphic nomenclature of Iranian oil consortium agreement area. AApG Bulletin 49, 2182-2245.

Koleini, M., 2012. Engineering geological assessment and rock mass characterization of the Asmari formation (Zagros range) as large dam foundation rocks in southwestern Iran. University of Pretoria.

Lacombe, O., Mouthereau, F., Kargar, S., Meyer, B., 2006. Late Cenozoic and modern stress fields in the western Fars (Iran): Implications for the tectonic and kinematic evolution of central Zagros. Tectonics 25, n/a-n/a.
Levandowski, W., Herrmann, R.B., Briggs, R., Boyd, O., Gold, R., 2018. An updated stress map of the continental United States reveals heterogeneous intraplate stress. Nature Geoscience 11, 433-437.
Lund, B., Townend, J., 2007. Calculating horizontal stress orientations with full or partial knowledge of the tectonic stress tensor. Geophysical Journal International 170, 1328-1335.
Maggi, A., Jackson, J., Priestley, K., Baker, C., 2000. A re-assessment of focal depth distributions in southern Iran, the Tien Shan and northern India: Do earthquakes really occur in the continental mantle? Geophysical Journal International 143, 629-661.
Mahbaz, S., Sardar, H., Namjouyan, M., Mirzaahmadian, Y., 2011. Optimization of reservoir cut-off parameters: a case study in SW Iran. Petroleum Geoscience 17, 355-363.
Martínez-Garzón, P., Kwiatek, G., Ickrath, M., Bohnhoff, M., 2014. MSATSI: A MATLAB package for stress inversion combining solid classic methodology, a new simplified user-handling, and a visualization tool. Seismological Research Letters 85, 896-904.
Mastin, L., 1988. Effect of Borehole Devition on Breakout Orientation. J Geophys Res 93, 9187-9195.
Mazidi Saber Mehrabi , Haftani Mohammad , Bohloli Bahman , Akbar, C., 2012. Measurement of uniaxial compressive strength of rocks using reconstructed cores from rock cuttings. Journalof Petroleum Science and Engineering 86, 39-43.
McGarr, A., Simpson, D., Seeber, L., Lee, W., 2002. Case histories of induced and triggered seismicity. International Geophysics Series 81, 647-664.
McKenzie, D., 1972. Active tectonics of the Mediterranean region. Geophysical Journal International 30, 109-185.
Michael, A.J., 1984. Determination of stress from slip data: faults and folds. Journal of Geophysical Research: Solid Earth 89, 11517-11526.
Mobasher, K., Babaie, H.A., 2008. Kinematic significance of fold- and fault-related fracture systems in the Zagros mountains, southern Iran. Tectonophysics 451, 156-169.
Molinaro, M., Leturmy, P., Guezou, J.C., Frizon de Lamotte, D., Eshraghi, S., 2005. The structure and kinematics of the southeastern Zagros fold-thrust belt, Iran: From thin-skinned to thick-skinned tectonics. Tectonics 24.
Moos, D.B., Zoback, M.D., 1990. Utilization of observations of well bore failure to constrain the orientation and magnitude of crustal stresses: application to continental deep sea drilling project and ocean drilling program boreholes. J Geophys Res 95, 9305–9325.
Morris, A., Ferrill, D.A., Henderson, D.B., 1996. Slip-tendency analysis and fault reactivation. Geology 24, 275-278.
Motiei, H., 1994. Stratigraphy of Zagros (In Farsi). Geological Survey of Iran.
Mouthereau, F., Lacombe, O., Tensi, J., Bellahsen, N., Kargar, S., Amrouch, K., 2007. Mechanical constraints on the development of the Zagros Folded Belt (Fars), Thrust Belts and Foreland Basins. Springer, pp. 247-266.
Nabaei, M., Moazzeni, A.R., Ashena, R., Roohi, A., 2011. Complete Loss, Blowout and Explosion of Shallow Gas, Infelicitous Horoscope in Middle East, SPE European Health, Safety and Environmental Conference in Oil and Gas Exploration and Production. Society of Petroleum Engineers.
Najibi, A.R., Asef, M.R., 2014. Prediction of seismic-wave velocities in rock at various confining pressures based on unconfined dataPrediction of seismic-wave velocities in rock at various confining pressures based on unconfined data. GEOPHYSICS 79, 235-242.
Najibi, A.R., Ghafoori, M., Lashkaripour, G.R., Asef, M.R., 2015. Empirical relations between strength and static and dynamic elastic properties of Asmari and Sarvak limestones, two main oil reservoirs in Iran. Journal of Petroleum Science and Engineering 126, 78-82.
Ni, J., Barazangi, M., 1986. Seismotectonics of the Zagros continental collision zone and a comparison with the Himalayas. Journal of Geophysical Research: Solid Earth 91, 8205-8218.

Nissen, E., Tatar, M., Jackson, J.A., Allen, M.B., 2011. New views on earthquake faulting in the Zagros fold-and-thrust belt of Iran. Geophysical Journal International 186, 928-944.
Peyret, M., Rolandone, F., Dominguez, S., Djamour, Y., Meyer, B., 2008. Source model for the Mw 6.1, 31 March 2006, Chalan-Chulan earthquake (Iran) from InSAR. Terra Nova 20, 126-133.
Pirouz, M., 2018. Post-collisional deposits in the Zagros foreland basin: Implications for diachronous underthrusting. International Journal of Earth Sciences 107, 1603-1621.
Pirouz, M., Simpson, G., Bahroudi, A., Azhdari, A., 2011. Neogene sediments and modern depositional environments of the Zagros foreland basin system. Geological Magazine 148, 838-853.
Plumb, R.A., Cox, J.W., 1987. Stress directions in eastern North America determined to 4.5 km from borehole elongation measurements. . J Geophys Res 90, 5513-5522.
Priestley, K., Baker, C., Jackson, J., 1994. Implications of earthquake focal mechanism data for the active tectonics of the South Caspian Basin and surrounding regions. Geophysical Journal International 118, 111-141.
Roth, F., Fleckenstein, P., 2001. Stress orientations found in north-east Germany differ from the West European trend. Terra Nova 13, 289-296.
Rudkiewicz, J.L., Sherkati, S., Letouzey, J., 2007. Evolution of maturity in Northern Fars and in the Izeh Zone (Iranian Zagros) and link with hydrocarbon prospectivity, Thrust Belts and Foreland Basins. Springer, pp. 229-246.
Salehi, M., Miri, A., Sherkati, S., Bahroudi, A., 2012. Analysis of pore pressure effect on abnormal thickness variation of Dashtak Fm. as a detachment layer in Fars region of Zagros fold and thrust belt, Istanbul 2012-International Geophysical Conference and Oil & Gas Exhibition. Society of Exploration Geophysicists and The Chamber of Geophysical …, pp. 1-4.
Sardar, H., Mahbaz, S.B., 2009. Rock physics modeling in sandstone member of Asmari reservoir (a case study from Mansuri oil field), SEG Technical Program Expanded Abstracts 2009. Society of Exploration Geophysicists, pp. 2203-2207.
Sarkarinejad, K., Zafarmand, B., Oveisi, B., 2017. Evolution of the stress fields in the Zagros Foreland Folded Belt using focal mechanisms and kinematic analyses: the case of the Fars salient, Iran. International Journal of Earth Sciences.
Schmitt, D.R., Currie, C.A., Zhang, L., 2012. Crustal stress determination from boreholes and rock cores: Fundamental principles. Tectonophysics 580, 1-26.
Sepehr, M., Cosgrove, J., 2004. Structural framework of the Zagros fold–thrust belt, Iran. Marine and Petroleum geology 21, 829-843.
Sepehr, M., Cosgrove, J.W., 2007. The role of major fault zones in controlling the geometry and spatial organization of structures in the Zagros Fold-Thrust Belt. Geological Society, London, Special Publications 272, 419-436.
Shen, L.W., Schmitt, D.R., Haug, K., 2019. Quantitative constraints to the complete state of stress from the combined borehole and focal mechanism inversions: Fox Creek, Alberta. Tectonophysics 764, 110-123.
Sherkati, S., Letouzey, J., 2004. Variation of structural style and basin evolution in the central Zagros (Izeh zone and Dezful Embayment), Iran. Marine and Petroleum Geology 21, 535–554.
Simpson, R.W., 1997. Quantifying Anderson's fault types. Journal of Geophysical Research: Solid Earth 102, 17909-17919.
Skirokova, E., 1967. General features in the orientation of principal stresses in earthquake foci in the Mediterranean-Asian seismic belt, Izv. Earth Phys, 22-36.
Snee, J.E.L., Zoback, M.D., 2016. State of stress in Texas: Implications for induced seismicity. Geophysical Research Letters 43, 10,208-210,214.
Soleimani, B., Hassani-Giv, M., Abdollahi fard, I., 2017. Formation Pore Pressure Variation of the Neocomian Sedimentary Succession (the Fahliyan Formation) in the Abadan Plain Basin, SW of Iran. Geofluids 2017, 13.
Sonder, L.J., 1990. Effects of density contrasts on the orientation of stresses in the lithosphere: Relation to principal stress directions in the Transverse Ranges, California. Tectonics 9, 761-771.

Talebi, H., Alavi, S.A., Sherkati, S., Ghassemi, M.R., Golalzadeh, A., 2018. In-situ stress regime in the Asmari reservoir of the Zeloi and Lali oil fields, northwest of the Dezful embayment in Zagros fold-thrust belt, Iran. فصلنامه علمی-پژوهشی علوم زمین 27, 53-68.

Talebian, M., Jackson, J., 2002. Offset on the Main Recent Fault of NW Iran and implications for the late Cenozoic tectonics of the Arabia–Eurasia collision zone. Geophysical Journal International 150, 422-439.

Talebian, M., Jackson, J., 2004. A reappraisal of earthquake focal mechanisms and active shortening in the Zagros mountains of Iran. Geophysical Journal International 156, 506-526.

Tatar, M., Hatzfeld, D., Ghafory-Ashtiany, M., 2004. Tectonics of the Central Zagros (Iran) deduced from microearthquake seismicity. Geophysical Journal International 156, 255-266.

Tingay, M., Bentham, P., De Feyter, A., Kellner, A., 2011. Present-day stress-field rotations associated with evaporites in the offshore Nile Delta. Bulletin 123, 1171-1180.

Townend, J., Zoback, M.D., 2000. How faulting keeps the crust strong. Geology 28(5), 399-402.

Walker, R.T., Andalibi, M.J., Gheitanchi, M.R., Jackson, J.A., Karegar, S., Priestley, K., 2005. Seismological and field observations from the 1990 November 6 Furg (Hormozgan) earthquake: a rare case of surface rupture in the Zagros mountains of Iran, Geophysical Journal International, pp. 567-579.

Walpersdorf, A., Hatzfeld, D., Nankali, H., Tavakoli, F., Nilforoushan, F., Tatar, M., Vernant, P., Chéry, J., Masson, F., 2006. Difference in the GPS deformation pattern of North and Central Zagros (Iran). Geophysical Journal International 167, 1077-1088.

Ward, C.D., Andreassen, E., 1997. Pressure while drilling data improves reservoir drilling performance. SPE 37588 In: SPE/IADC Drilling Conference, Amsterdam.

Wessel, P., Smith, W.H., 1998. New, improved version of Generic Mapping Tools released. Eos, Transactions American Geophysical Union 79, 579-579.

Yaghoubi, A.A., Zeinali, M., 2009. Determination of magnitude and orientation of the in-situ stress from borehole breakout and effect of pore pressure on borehole stability—Case study in Cheshmeh Khush oil field of Iran. Journal of Petroleum Science and Engineering 67, 116-126.

Yamini-Fard, F., Hatzfeld, D., Tatar, M., Mokhtari, M., 2006. Microearthquake seismicity at the intersection between the Kazerun fault and the Main Recent Fault (Zagros, Iran). Geophysical Journal International 166, 186-196.

Yang, W., Hauksson, E., 2013. The tectonic crustal stress field and style of faulting along the Pacific North America Plate boundary in Southern California. Geophysical Journal International 194, 100-117.

Zarifi, Z., Nilfouroushan, F., Raeesi, M., 2014. Crustal stress map of Iran: insight from seismic and geodetic computations. Pure and Applied Geophysics 171, 1219-1236.

Zoback, M.L., 1992. First and Second Order Patterns of Tectonic Stress: the World Stress Map Project. J Geophys Res 97, 11703–11728.

Figure 1.

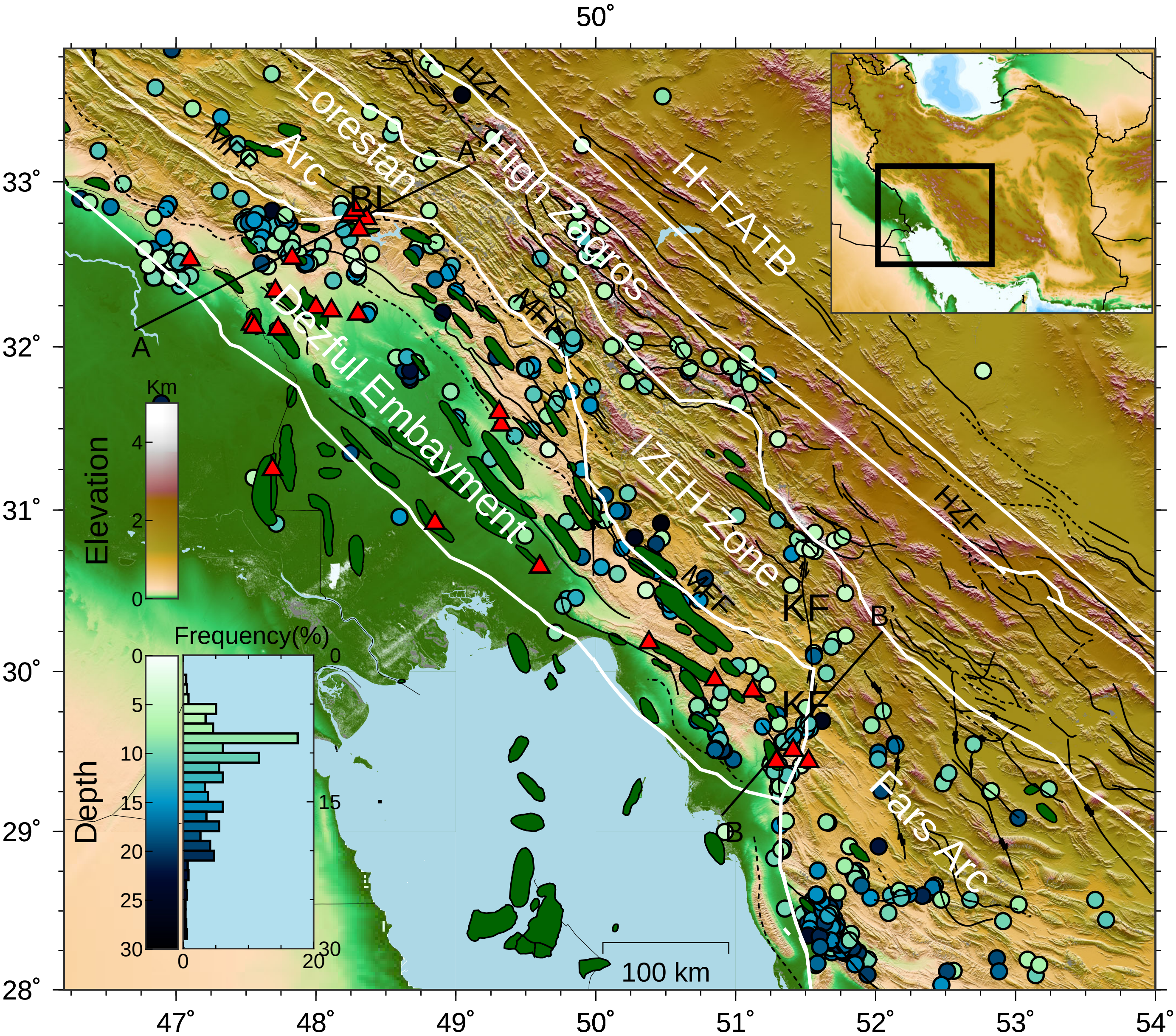
50°
33°
32°
31°
30°
29°
28°
47°
48°
49°
50°
51°
52°
53°
54°
HZF
MFF
Lorestan
Arc
A'
BL
High Zagros
H-FATB
MFF
A
Dezful Embayment
Km
Elevation
IZEH Zone
HZF
MFF
KF
B'
Frequency(%)
KF
Depth
Fars Arc
B
100 km

Figure 2.

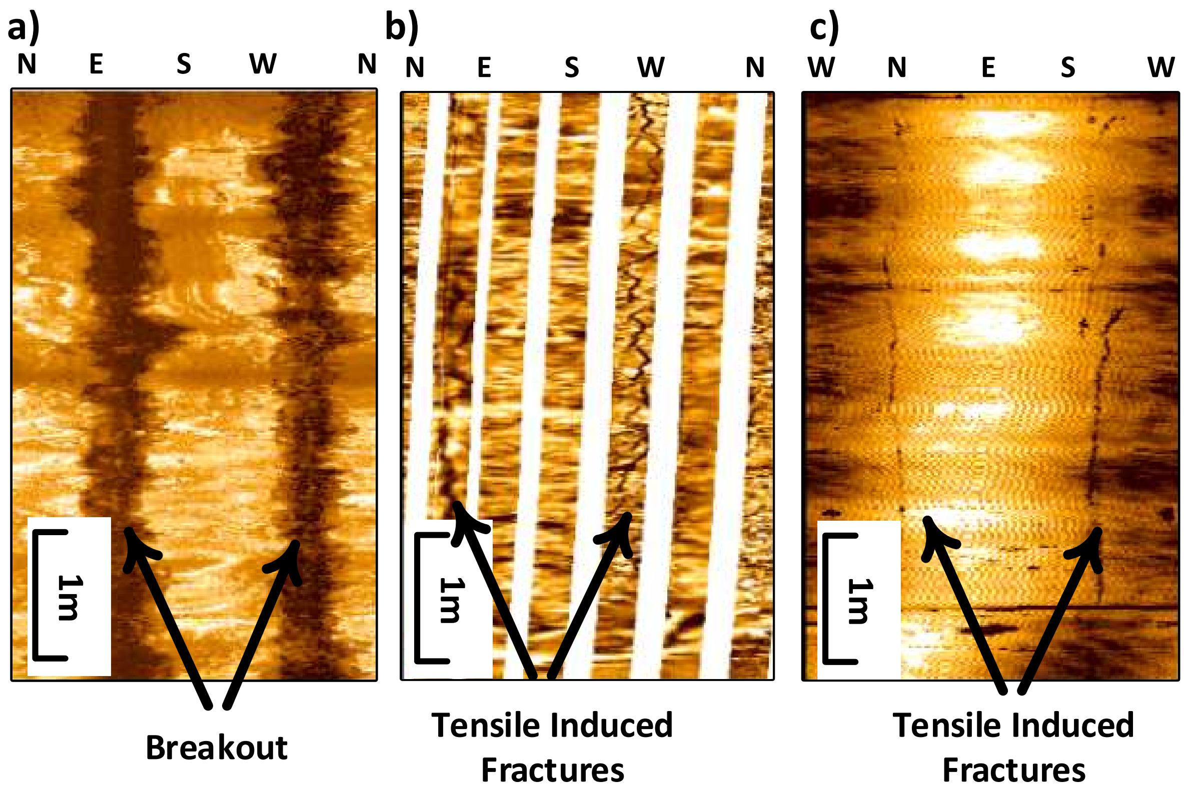

Figure 2: Examples of borehole breakout in a) the E-W direction in the Dehloran oil field (4150 m) and b) tensile induced fracture in NE-SW direction in the Khesht oil field (2880 m), and c) one in the N-S direction in the Paydar oil field (3210 m).

Figure 3.

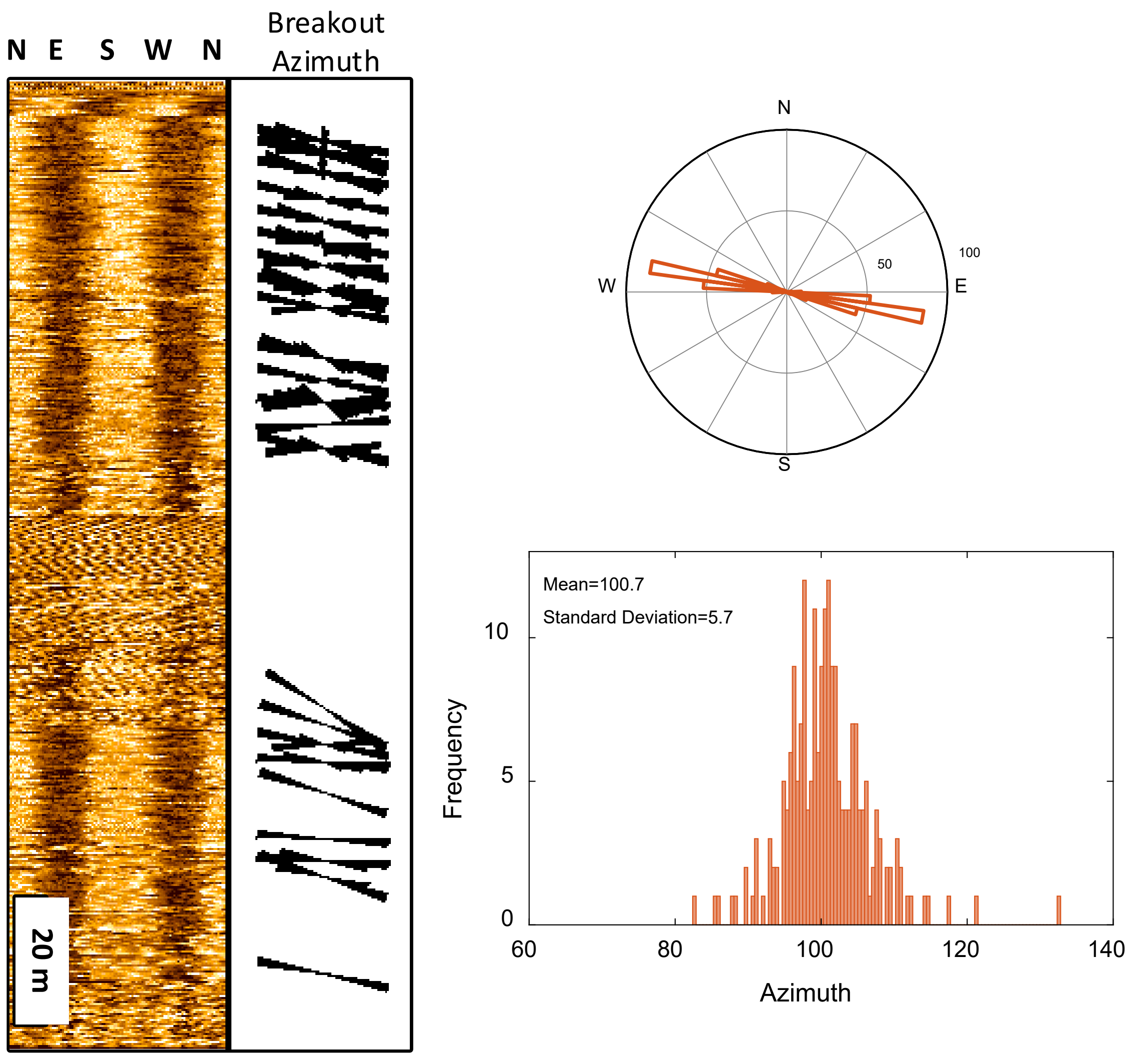

Figure 3: UBI log indicates that the minimum principal direction (borehole breakout) is 100°±5.7° in Well 7 of the West Paydar field.

Figure 4.

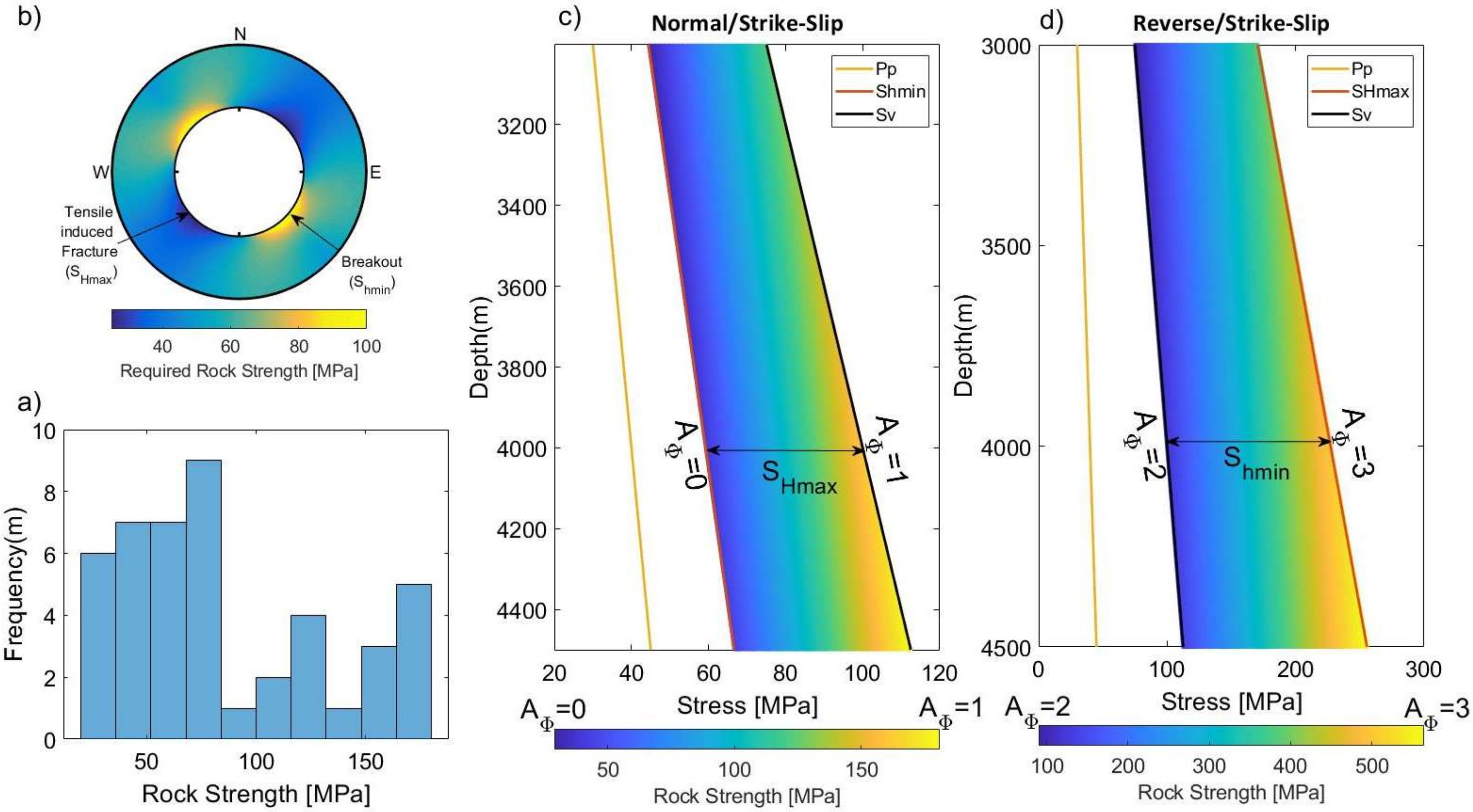

Figure 4: b) The uniaxial compressive rock strength (UCS) histogram of limestone in the Sarvak and Asmari Formations of the Mansori field; b) example of stress concentration around a vertical borehole and the location of borehole breakout and tensile induced fracture and their relation to principal stress orientations;. c) and d) rock strength required to initiate a breakout in normal and reverse faulting regimes in the Sarvak and Asmari Formations of the DE, assuming that the stresses at the limit are constrained by a friction coefficient μ = 0.6, P_p = 10 MPa/km, and S_v = 26 MPa/km (equation (1)). The color bar shows rock strength needed to prevent borehole breakout in vertical boreholes. Mohr–Coulomb failure criterion and Kirsch equations (equation (2)) were used in these calculations.

Figure 5.

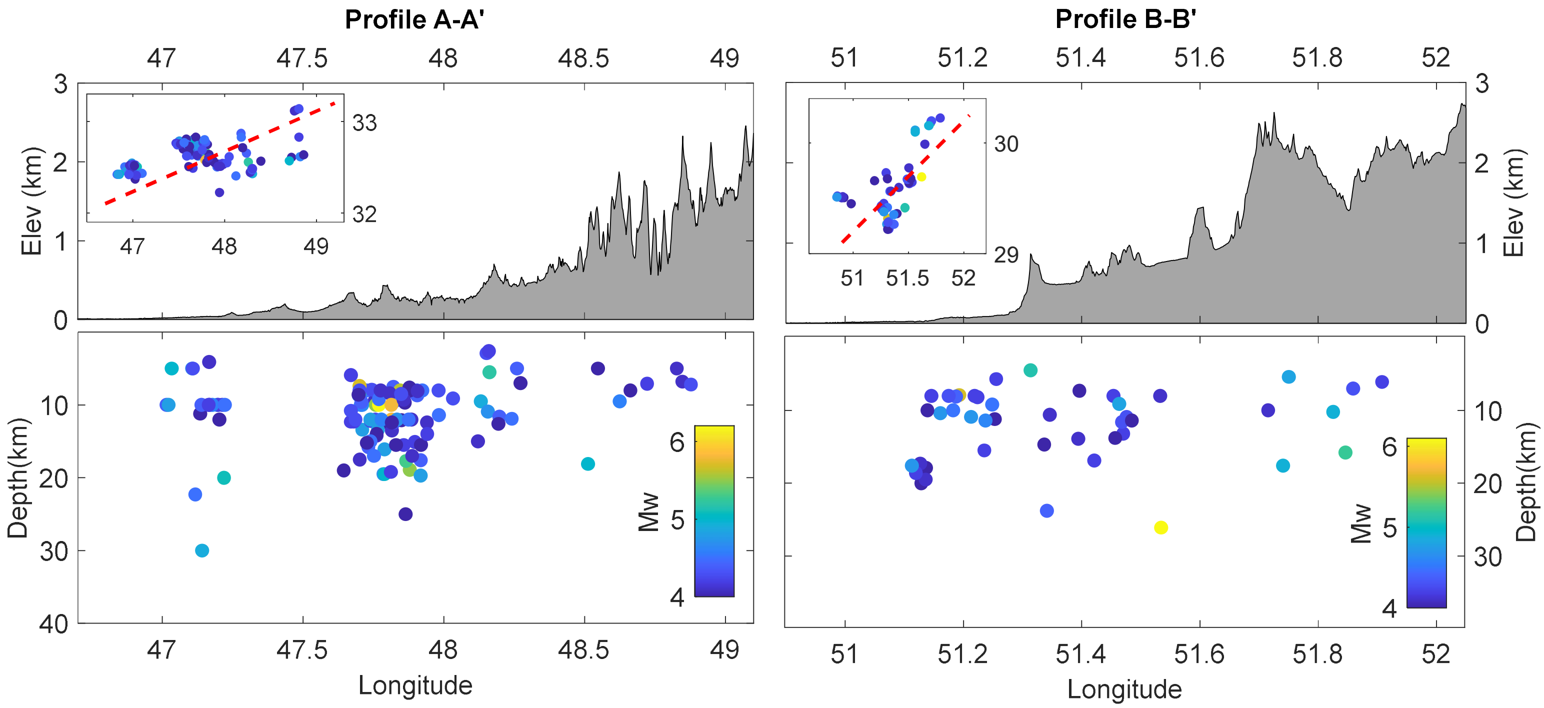

Figure 5: Cross-sections of DE displaying topography and seismicity in A-A’ and B-B’ sections shown in Figure 1. The colour scale represents earthquake magnitudes. The high seismicity density in the area is restricted to below 4 km. Details of each earthquake are provided in the supplementary materials (Table S2).

Figure 6.

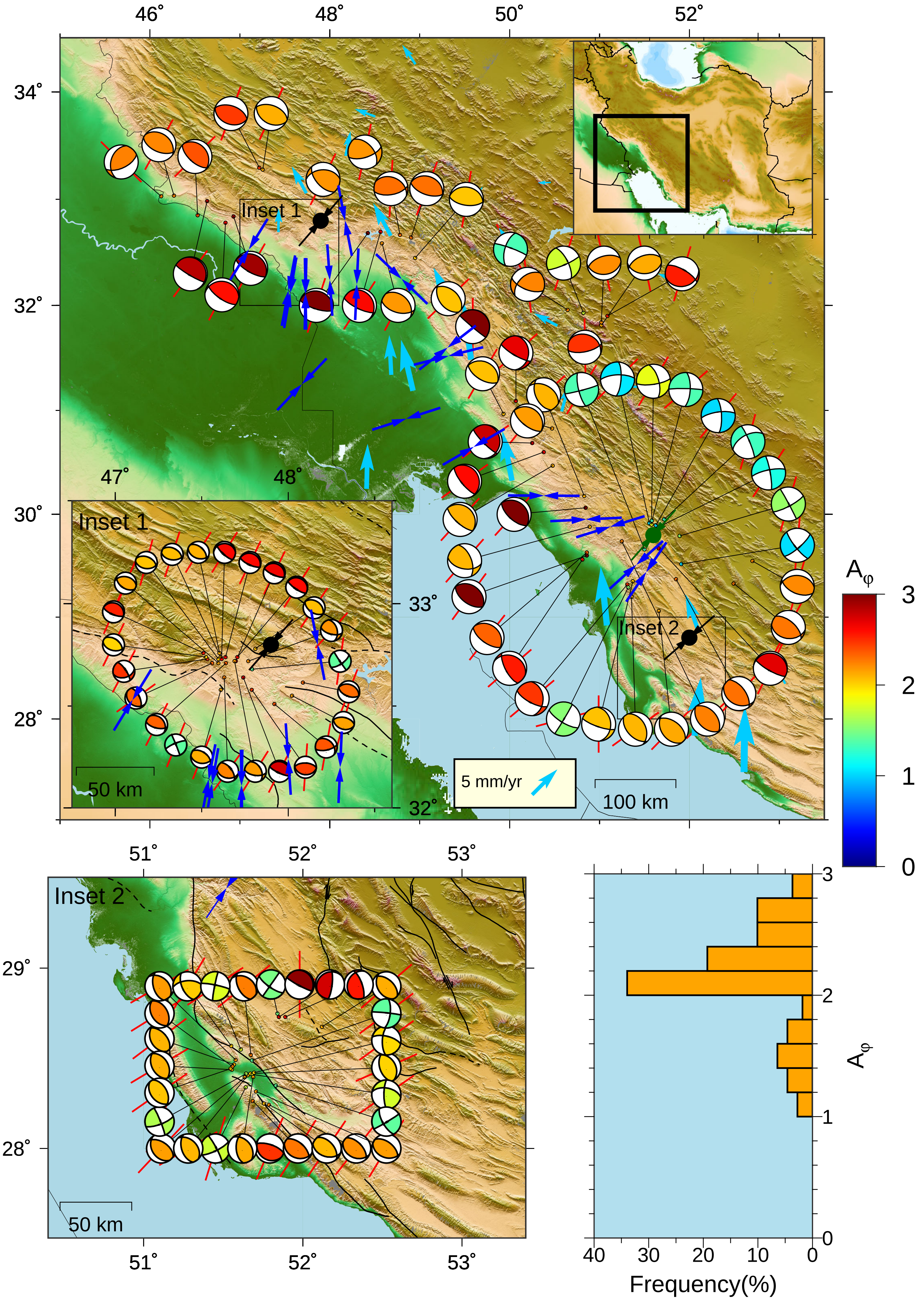
46°
48°
50°
52°
34°
32°
30°
28°
Inset 1
Inset 2
47°
48°
33°
32°
50 km
5 mm/yr
100 km
A_φ
3
2
1
0
51°
52°
53°
29°
28°
50 km
Frequency(%)
40
30
20
10
0

Figure 7.

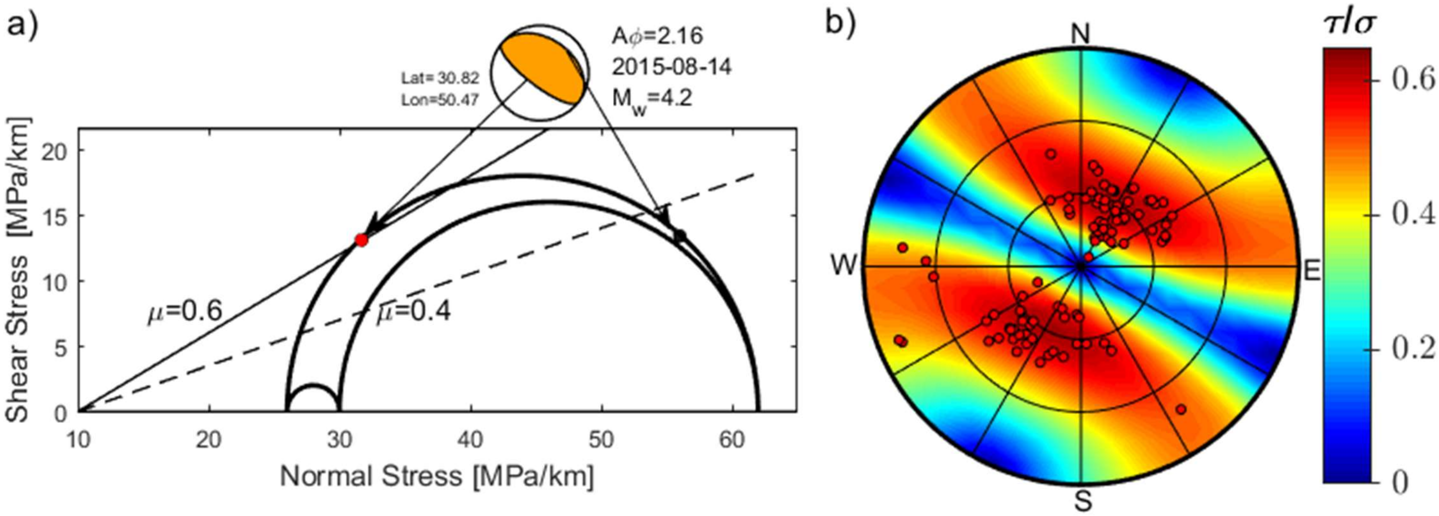

Figure 7: a) 3D Mohr's circle showing representative reverse focal plane mechanisms and resolved shear and normal stresses for each nodal plane. The color inside the beach ball represents A_{ϕ} and is based on the color bar shown in Figure 6. b) Lower hemisphere stereonet plot of the preferred nodal plane for 92 focal plane mechanisms in the DE where the state of stress is a thrust-faulting regime. Colors show the ratio of shear to effective normal stresses (required μ) needed for shear failure on a fault plane.

Figure 8.

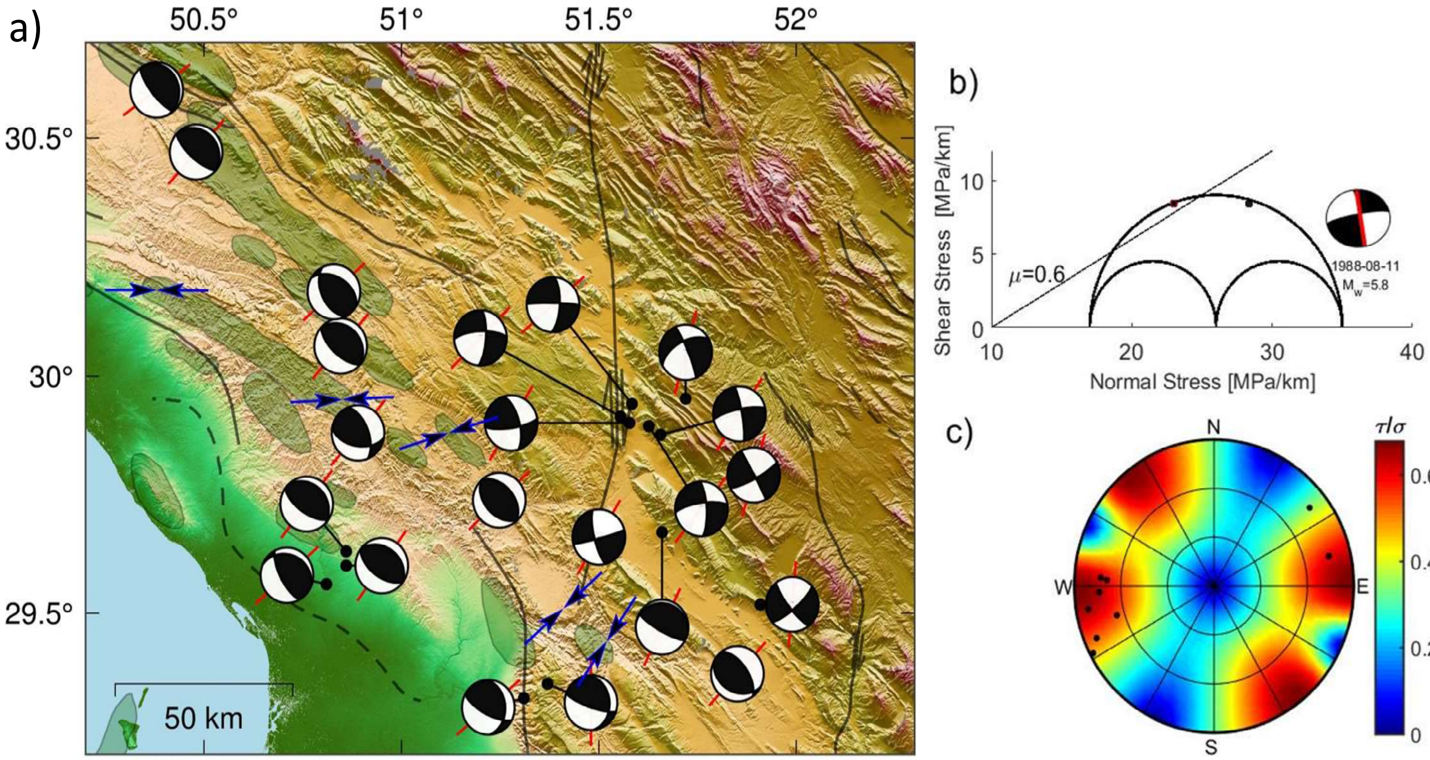

Figure 8: a) Earthquake focal mechanisms in the vicinity of the N-S Kazerun transverse active fault. The state of stress changes from strike-slip faulting around the fault to a reverse faulting regime on either side whereas the seismologically (red line) determined azimuth S_{Hmax} (P-Axis) is stable and uniform around the area. b) 3D Mohr's circle showing a representative strike-slip focal plane mechanism and resolved shear and normal stresses for each nodal plane. The red line on the focal beach-ball indicates the actual fault plane. c) Lower hemisphere stereonet plot illustrates the slip-tendency (ratio of resolved shear to normal stress) associated with the strike-slip Kazerun fault and actual nodal plane for 12 focal plane mechanisms mapped in (a).

Figure 9.

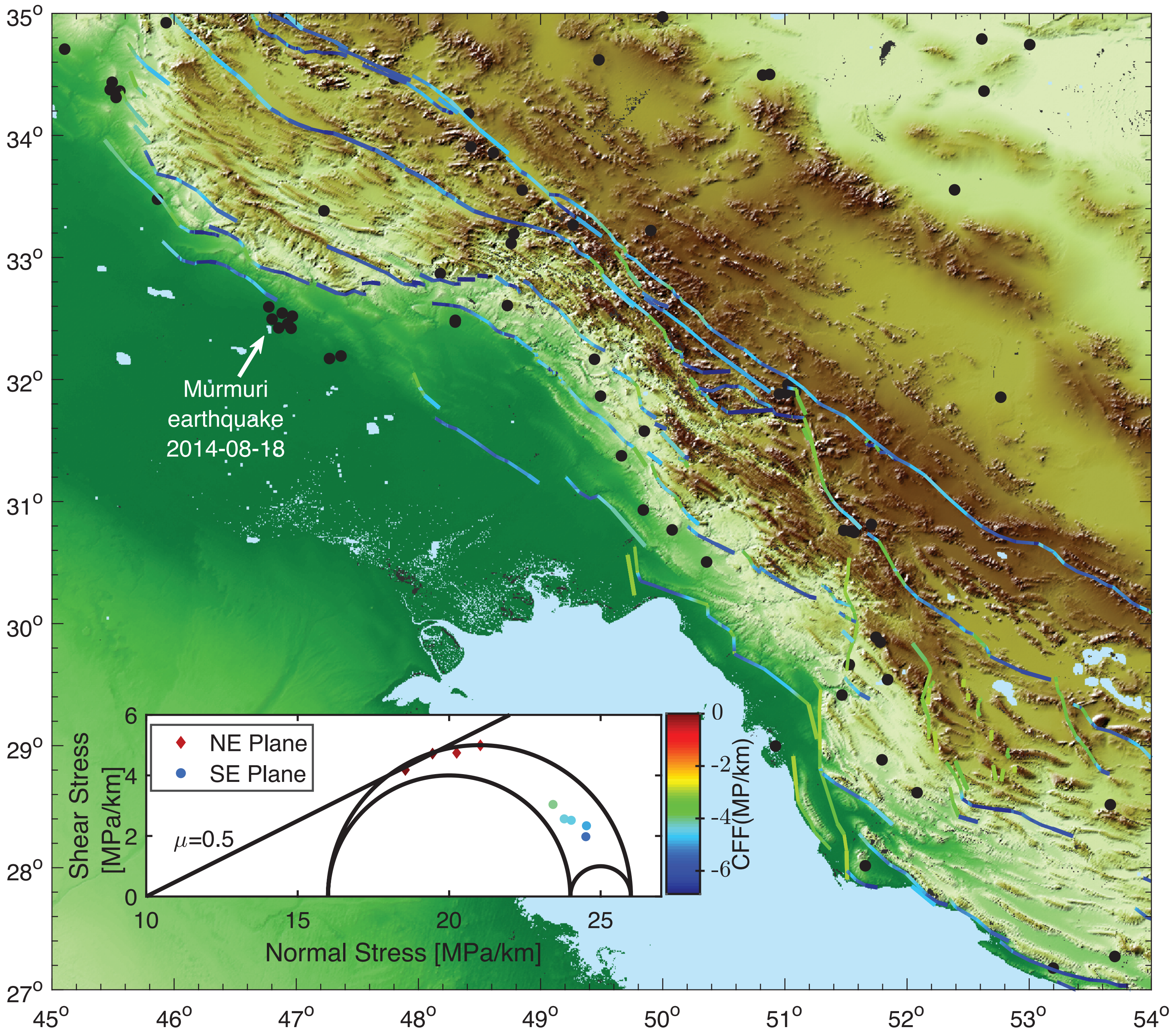

35°
34°
33°
32°
31°
30°
29°
28°
27°
45°
46°
47°
48°
49°
50°
51°
52°
53°
54°
Murmuri
earthquake
2014-08-18
NE Plane
SE Plane
μ=0.5
Shear Stress [MPa/km]
Normal Stress [MPa/km]
CFF(MP/km)
0
-2
-4
-6
0
2
4
6
10
15
20
25

Table 1: S_{Hmax} orientations by quality ranking derived from both borehole breakout (BO) and drilling induced fracture (DIF) in the different fields in the DE.

Field	Well Name abbreviation	Latitude	Longitude	S_{Hmax} Azimuth (deg)	Type	Number	Total length (m)	Depth (m)	Orientation (deg.)	S.D.	WSM (quality)
Aghajari	AJ-215	30.69	43.86	32	BO	5	110	2475	122	7.3	C
Balarud	BL-2	32.8	48.25	147.6	BO	6	140	2243	57.6	2.1	B
	BL-2	32.8	48.25	152.5	DIF	6	464	2174	152.5	11.1	B
	BL-3	32.78	48.36	175	BO	1	---	1616	85	----	D
	BL-3	32.78	48.36	174.9	DIF	10	269	1805	174.9	20	B
	BL-4	32.83	48.28	42.9	BO	19	503	1846	132.92	19.9	B
	BL-4	32.83	48.28	109.9	DIF	3	18	1705	109.9	18.6	D
	BL-6	32.71	48.31	169.08	DIF	24	623	1934	169.08	12.9	A
Bibi-Hakimih	BH-177	29.95	50.85	87.2	BO	51	210	1972	177.2	11.6	A
	BH-179	30.18	50.38	90.3	BO	109	520	2121	180.3	10.8	A
Chahar Bisheh	CB-4	29.88	51.12	52	BO	149	295	1953	142.0	9.9	A
Cheshmeh-khosh	CK-8	32.24	48.00	176	BO	25	238	3548	86.00	4.2	A
	CK-9	32.34	47.71	75	BO	43	221	4172	165.00	26.0	C
	CK-22	32.20	48.30	182.6	BO	10	106	3522	92.6	6.9	A
Dalpari	DP-08	32.54	47.83	157.3	BO	30	150	2340	67.3	32.1	D
Dehloran	DH-23	32.53	47.1	31.4	BO	52	415	4164	121.4	7.14	A
Khesht	KH-2	29.51	51.41	138	BO	28	402	2810	48.0	9.8	A
	KH-2	29.51	51.41	142.75	DIF	4	191	2845	322.75	8.7	C
	KH-5	29.44	51.29	124.05	BO	36	197	2994	34.05	8.7	A
	KH-5	29.44	51.52	119.4	DIF	19	215	2984	299.4	17.8	B
Lali	LL-22	32.25	134.2	44.2	BO	35	230	2278	44.2	11.2	A
	LL-29	32.22	48.11	135	BO	158	466	2547	46.10	43.3	E
Mansouri	MI-99	30.92	48.85	72.02	BO	22	179	3259	162.02	5.02	A
Maroun	MN446	31.524	49.324	75.7	BO	167	125	4293	165.70	5.3	A
Naft_Sefied	NS-47	31.60	49.31	72.75	BO	29	270	1625	162.75	9.78	A
Paydar	P-2	32.11	47.73	1.3	BO	89	681	3304	91.30	6.8	A
	P-2	32.11	47.73	179.2	DIF	99	576	3294	179.2	20.3	A
	P-6	32.14	47.54	10.7	BO	213	310	4045	100.7	5.7	A
	P-7	32.12	47.56	9.8	BO	135	230	4035	99.8	6.2	A
Ramshir	RR-19	30.65	49.6	59.65	BO	32	248	3061	149.65	6.70	A
	RR-19	30.65	49.6	70.8	DIF	3	48	2818	70.8	3.9	D
Yaran	YRRN-2	31.25	47.69	43.6	BO	11	140	3980	133.60	7.5	A

Table 2: Stress inversion results at different locations in the DE.

Lat (°N)	Long (°W)	Number of Focal Mechanisms	S1 Azimuth (°)	S1 Plunge (°)	R=(1-φ)	Faulting Regime
48	33	68	205	4.1	0.72±0.2	R
52	29	31	223	5.7	0.78±0.25	R
51.6	29.8	23	221	4.3	0.84±0.15	S